Rivista Italiana di Paleontologia e Stratigrafia
(*Research in Paleontology and Stratigraphy*)
vol. 131(2): 281-304. **July 2025**
DOI: https://doi.org/10.54103/2039-4942/24033

BENTHIC ECOSYSTEM VARIATIONS ALONG THE MIDDLE EOCENE PROVENÇAL DROWNING RAMP

VICTOR MANUEL GIRALDO-GÓMEZ[1,2], ANTONINO BRIGUGLIO[1]*, ANDREA BAUCON[1], CESARE ANDREA PAPAZZONI[3], JOHANNES PIGNATTI[4], ANTONELLA GANDOLFI[1] & MICHELE PIAZZA[1]

[1]Dipartimento di Scienze della Terra, dell'Ambiente e della Vita, Università degli Studi di Genova, Corso Europa 26, 16132 Genova, Italy. Email: antonino.briguglio@unige.it
[2]Ellington Geological Services, 1414 Lumpkin Rd, 77043 Houston, USA.
[3]Dipartimento di Scienze Chimiche e Geologiche, Università di Modena e Reggio Emilia, Via Campi 103, 41125 Modena, Italy.
[4]Dipartimento di Scienze della Terra, Università degli Studi di Roma "La Sapienza", Piazzale Aldo Moro 5, 00185 Roma, Italy.
*Corresponding author

Associate Editor: Francesca Bosellini.

To cite this article: Giraldo-Gómez V.M., Briguglio A., Baucon A., Papazzoni C.A., Pignatti J., Gandolfi A. & Piazza M. (2025) - Benthic ecosystem variations along the Middle Eocene Provençal drowning ramp. *Rivista Italiana di Paleontologia e Stratigrafia*, vol. 131(2): 281-304.

Keywords: Bartonian; microfacies; trace fossils; larger benthic foraminifera; spectral gamma-ray; shallow water; paleoenvironment; Ligurian Alps.

Abstract. High-resolution lithology, fossil content, ichnofabrics, and spectral gamma-ray emissions are studied in the Capo Mortola section in the Liguria region (NW Italy), correlating it with other middle Eocene (Bartonian) sections in the same region. The succession unconformably overlies Upper Cretaceous open-marine deposits and records a deepening trend on a carbonate ramp during the middle Eocene. Six different microfacies have been recognized, recording the variation in fossil content, especially in the larger benthic foraminiferal assemblages, and lithology, which indicate a deepening trend in the succession. The variation in Th/U ratios, measured by gamma ray emissions along the section, allows for differentiation of oxidizing, normal, and reducing conditions throughout the succession. The increase in the concentration of Th and K suggests periods of increased terrigenous material, which was supplied by a fluvial system close to the studied section. In turn, the Th/K ratio shows an alternation between smectite and kaolinite, which are respectively associated with warm-humid and seasonal humid/dry climates. The upper part of this section shows the incipient drowning of the ramp, which correlates with nearby studied sections; nonetheless, biotic components, lithology, and depositional depth differ in all localities due to the specific paleogeographic portion of the ramp. We were able to identify sectors more prone to seafloor instabilities due to their proximity to the shoreline and the deltaic influence, whereas others were located considerably deeper or farther out with respect to the input of deltaic sediments.

Introduction

In mixed carbonate-siliciclastic deposits, the understanding of sediment provenance and depositional rate is crucial, because they control the abundance and diversity of both meso- to eutrophic heterotrophic taxa (such as many smaller benthic foraminifera, oysters, and other bivalves, and gastropods) and mainly oligotrophic, mixo- to autotrophic taxa (such as corals and larger benthic foraminifera) that thrive usually in oligotrophic waters (e.g., Hallock & Schlager 1986; Allmon 1988;

Received: July 9, 2024; accepted: April 10, 2025

Lokier et al. 2009; Moussavou 2015; Toscano et al. 2018).

Seasonal or episodic input of terrigenous material exerts a control over nutrients and suspended sediment that has a strong impact on the development of specific ecological niches for a large variety of taxa. Larger benthic foraminifera (LBF) host photosynthetic microalgae that are sensitive to seafloor irradiation instabilities, and their sudden abundance or disappearance along a succession can be related to a decrease or an increase in water turbidity (Hallock & Glenn 1986; Egger et al. 2013; Goeting et al. 2018; Renema 2018). In mixed carbonate-siliciclastic settings, turbidity can be triggered by intermittent inputs of siliciclastic sediments from the hinterland (Hottinger 1983; Hallock 1985, 2000; Hallock & Schlager 1986). The sensibility of larger benthic foraminifera to sea floor irradiation is routinely used as a proxy to reconstruct the bathymetry and ecological conditions of shallow water successions where they are abundant, especially during selected time intervals of the Paleozoic, Mesozoic, and the entire Cenozoic (Egger et al. 2017; Torres-Silva et al. 2017, 2019).

The Capo Mortola succession records the development of a carbonate ramp (Varrone & d'Atri 2007; Brandano 2019; Coletti et al. 2021; Marini et al. 2022) that underwent drowning and therefore has the potential to preserve shallow water benthic taxa as well as planktonic components. Such depositional scenario can permit the observation of how different species reacted to local and global climatic instabilities along an ecological gradient. Several studies in the region allow us to constrain the evolution of the carbonate ramp to be determined in detail, as well as the recognition of specific biota developments in the drowning system (e.g., Coletti et al. 2021; Brandano & Tomassetti 2022; Briguglio et al. 2024).

The Capo Mortola section was first studied by Carbone et al. (1980) who recognized different facies in the carbonate-terrigenous sequence of the middle Eocene but did not report climate-driven signals. Brandano (2019) described drowning dynamics in carbonate platforms from several sections of the Western Ligurian Alps and the Central Apennines (Italy), and concisely referred to the characteristics of the Bartonian Capo Mortola section to be possibly related to middle Eocene climatic dynamic. Coletti et al. (2021) reinterpreted the data of Carbone et al. (1980), providing a paleoenvironmental reconstructions of the Capo Mortola and some other sections, with a focus on terrigenous input and the contribution of coralline algae, excluding clear evidence of climatic perturbations.

The relationship between the Th/U and Th/K ratios, derived by spectral gamma-ray analyses, is used to assess depositional environments and paleoclimate conditions. Due to the strong link between changes in depositional environments and sedimentary processes, the Th/U ratio is a useful proxy for indicating paleoredox conditions (e.g., Adams & Weaver 1958; Wignall & Twitchett 1996; Basu et al. 2009; Kouamelan et al. 2020), and the Th/K ratio is linked by identifying the dominant clay minerals, which mirror paleoclimatical variations (Myers 1987; Myers & Wignall 1987; Bessa 1995; Ruffell & Worden 2000; Gao et al. 2018; Kouamelan et al. 2020).

The middle Eocene was a transitional interval in the Earth's climatic history, when global temperatures underwent considerable changes, characterized by the beginning of the shift from a greenhouse to an icehouse climate, the latter established in the early Oligocene (Zachos et al. 2008). This overall cooling trend was interrupted by a short-lived episode of worldwide warming during the middle Eocene (Middle Eocene Climatic Optimum, MECO). During the MECO, temperature increased between 3 and 6 °C, as shown by the negative $\delta^{18}O$ excursion of about 1‰ in marine carbonate sediments. This event lasted 400 kyr, having its maximum peak about 40 Ma, returning to the previous conditions (Zachos et al. 2001; Bohaty & Zachos 2003; Bohaty et al. 2009; Sluijs et al. 2014).

The aims of this study are: (1) to describe the textural variations of the mixed carbonate-siliciclastic deposits, recording their respective microfacies; (2) to infer the paleoclimate according to data from the spectral gamma-ray emissions; (3) to determine the diversity and abundance of the benthic and the planktonic fauna, along with ichnofabric characteristics, allowing the identification of possible environmental and paleoclimatical changes; and (4) to attempt the correlation of this mixed carbonate-siliciclastic succession on a regional scale within the French-Italian Maritime Alps to observe climatic controls during the deepening trend.

Geological setting

The Capo Mortola promontory (43°46'50.5" N - 7°33'20.8" E) is located just east of the Italy-France border and flanks the Hanbury Botanical Gardens (Fig. 1 A, B). Capo Mortola and the related submarine part of the promontory are included in the Hanbury Botanical Gardens Regional Protected Area. The Capo Mortola sedimentary succession is part of the south-eastern Provençal paleogeographic domain (Arc de la Roya, Southern Subalpine Chain, European Plate).

The stratigraphic succession starts with deep marine marls and marly limestones (Trucco Formation, Santonian–lower Maastrichtian), unconformably overlain by shallow marine, siliciclastic, mixed, and carbonate deposits (Capo Mortola Calcarenite = Nummulitic Limestone, lower Bartonian). A lag deposit containing extrabasinal clasts and *Microcodium* fragments marks the basal surface of the Capo Mortola Calcarenite. The stratigraphic succession grades upwards to hemipelagic silty marls and marls with interbedded sandstone beds (Olivetta San Michele Silty-Marl = Globigerina Marls, Bartonian–lower Priabonian). These beds are overlain by siliciclastic turbidite deposits (Ventimiglia Flysch) dated as late Bartonian–early Priabonian (Brandano 2019; Coletti et al. 2021; Marini et al. 2022; Briguglio et al. 2024; Arena et al. 2024; Giraldo-Gómez et al. 2024).

The thrusting of the Ligurian Alps orogenic wedge onto the European plate resulted in a peripheral foreland basin with the deposition of the Boussac's marine "Priabonian Trilogy", named "Nummulitique" by Lanteaume (1968) and revised by Sinclair (1997; "Sinclair underfilled trinity"). This sedimentary succession consists of shallow-water limestones grading to deep-water marls later covered by siliciclastic turbidite sedimentation in a ramp setting (Boussac 1912; Lanteaume 1968; Sinclair 1997; Varrone 2004; Giammarino et al. 2009, 2010; de Graciansky et al. 2010; Dallagiovanna et al. 2012a, b; Marini et al. 2022; Morelli et al. 2022).

The Capo Mortola section was measured along the western limb of the narrow, non-cylindrical syncline of Capo Mortola where the transgressive facies of the Capo Mortola Calcarenite resting on the weathered marly limestones of the Trucco Formation are well exposed (Fig. 1 C-F). In this section, the Olivetta San Michele Silty-Marl is poorly exposed, whereas the Ventimiglia Flysch and Microcodium Formation cannot be observed (Gèze et al. 1968; Lanteaume 1968; Carbone et al. 1980; Dallagiovanna et al. 2012a, b; Coletti et al. 2021).

Materials and methods

For the study of the Capo Mortola section (CM; Fig. 1), a 49.30-m-thick sedimentary succession was measured, and 52 rock samples (from CMW-1 to CM-48; Fig. 2) were collected. Samples labeled CMW refer to the lowermost part of the section, which is exposed along a small beach west of the Capo Mortola promontory, whereas CM refers to samples collected directly on the promontory (Fig. 1 B, C, E, F, G, and H).

Lithology was determined using the carbonate classification systems of Grabau (1904) and Flügel (2012), identifying at the outcrop three main granulometric terms: calcisiltite, calcarenite, and calcirudite. One hundred and nine thin sections were prepared and analyzed to determine the biogenic, carbonate and siliciclastic components, as well as the matrix. Thin sections were analyzed on a custom-made Optech GZ808 optical stereomicroscope, and photos were taken with a Delta Pix Invenio (6EIII) digital camera.

Microfacies were described according to Dunham´s (1962) classification, and the biotic components were identified at family level or higher. Larger benthic foraminifera (LBF) were identified to genus level when possible. For thin section analysis, the matrix was estimated using charts that describe the percentage of grains in the limestones (Baccelle & Bosellini 1965): 1) matrix percentage (0: 0%; 1: 1-10%; 2: 11-50%; 3: >50%); 2) grain roundness and grain sorting (0: poor; 1: well; 2: very well); 3) grain size (see Flügel 2012: 0: fine; 1: medium; 2: coarse); 4) presence of quartz, glauconite, and organic matter (0: absent; 1: common; 2: abundant); 5) taxonomic diversity including nummulitids (separating *Nummulites* and *Assilina*), *Operculina*, orthophragmines, smaller benthic foraminifera, planktonic foraminifera, mollusks, calcareous algae, corals, echinoderms, and worm tubes (0: absent; 1: common; 2: abundant); and 6) additional features such as diagenesis (e.g., cements), bioturbation, deformation, and transport evidence (0: absent; 1: common; 2: abundant) (See Supplementary material Table S1 for more detail). These data were analyzed by cluster analysis using Ward's method (Ward 1963) and the Past software (Hammer et al. 2001).

LBF are very abundant and visible both on the field and in thin sections. Among them, nummulitids are the most abundant; they are mostly recorded in random oblique or axial sections and therefore they were identified using the taxonomic concepts of Kleiber (1991). For specimens observed along their equatorial plane, Schaub's (1981) monograph was followed.

All samples and thin sections are stored in the collections of the University of Genova (Dipartimento di Scienze della Terra, dell'Ambiente e della Vita; DISTAV).

Spectral gamma ray (SGR) was measured along the Capo Mortola section (sample average distance was 37 cm) using a Codevintec Gamma Ray Surveyor Vario (VN6 NaI (Ti)). The abundances of uranium (ppm), thorium (ppm), potassium (%), and the gamma-ray dose rate (DR nGy/h) were measured from 129 detections (lasting 3 minutes per detection) through the section. Radioactivity emitted by potassium (K), uranium (U), and thorium (Th) provides the natural gamma ray count concentration in rocks, which can be measured non-destructively and in real time, both in an outcrop and in a borehole (Slatt et al. 1992; Ruffell & Kürschner 2020). High Th/U ratios are interpreted as indicating a higher continental input of the sediment (Th/U >7) and are associated with oxidizing

conditions, whereas low values (Th/U <2) are related to low to none continental origin of the sediment and are associated with reducing conditions (anoxic). Transitional periods between oxidizing and reducing environments, associated with normal conditions (in oxic to dysoxic settings), are represented in marine settings by Th/U ratios ranging from 2 to 7 (e.g., Cowan & Myers 1988; Wignall & Twitchett 1996; Dypvik & Harr 2001; Basu et al. 2009; Kouamelan et al. 2020; Cao et al. 2021).

The thorium-potassium ratio (Th/K) was calculated to determine the type of clay mineral content (e.g., Schlumberger 1997); this can change along sedimentary successions especially when influenced by deltaic activities (Myers 1987; Myers & Wignall 1987; Bessa 1995; Ruffell & Worden 2000; Gao et al. 2018; Kouamelan et al. 2020). Analysis of the Th/K ratio was previously compared with results from XRF (X-ray fluorescence spectrometry) and XRD (X-ray diffraction) to assess the content of clay minerals (e.g., XRF: Ruffell & Worden 2000; Day-Stirrat et al. 2021; and XRD: Deconinck et al. 2003; Schnyder et al. 2006; Hesselbo et al. 2009; Paredes et al. 2020; Reolid et al. 2020).

Based on the multidisciplinary workflow of Crippa et al. (2018), we integrated the study of body fossils (i.e., mollusks, echinoderms, and foraminifera) with the analysis of distinct trace fossils and ichnofabrics. The Capo Mortola outcrops lack sufficiently wide bedding planes, which presents challenges in fully examining trace fossils in horizontal orientation. For this reason, bioturbation at Capo Mortola was studied in cross-section on vertical rock exposures, where ichnofabrics could be easily observed. Consequently, emphasis was placed on textural aspects that arise from biological reworking, i.e., ichnofabrics (Ekdale & Bromley 1983; Taylor et al. 2003).

The description and interpretation of ichnofabrics were based on outcrop observations. The spacing between successive observations was less than 1 m. Each of the observed areas, measuring approximately 50x50 cm, was ascribed to an ichnofabric class distinguished according to: (1) the degree of bioturbation, quantified as percent of the bioturbated area (Knaust 2021); (2) components of the ichnofabric, including either distinct trace fossils or bio-deformational structures with indistinct outlines (Taylor et al. 2003; Wetzel & Uchman 1998); (3) ichnodiversity, i.e., number of ichnotaxa present; and (4) the vertical distribution of bioturbation. Following standard ichnological practice (Bromley 1996; Taylor et al. 2003; Gingras et al. 2011; Knaust 2017), relative abundance, burrow size, tiering, and trace fossil frequency were also observed. Ichnotaxa were identified at the ichnospecies level whenever possible.

Results

Description of the Capo Mortola section

The base of the Capo Mortola section belongs to the Trucco Formation (Upper Cretaceous), characterized by alternating middle- to dark-grey marls and marly limestones beds (dipping NW 35°/75°). The unconformity that separates the Upper Cretaceous beds from the Eocene calcarenite is characterized by frequent borings into the Cretaceous substrate, in which Eocene nummulitids occur.

The Capo Mortola Calcarenite (middle Eocene) has a thickness of 46.46 m in this section and consists of marly limestones (calcisiltite, calcarenite, calcirudite, biocalcisiltite, biocalcarenite, and biocalcirudite; Figs. 1 F, G, H, and 2). The succession starts with deep-water Upper Cretaceous globotruncanid-rich limestone marked at the top by a regional unconformity that is characterized by black chert pebbles, conglomeratic lenses, thick agamonts (microspheric forms) of *Nummulites perforatus* (Montfort, 1808). Several ichnofossils (*Gastrochaenolites* sp.) are associated with the unconformity. Further up-section, three layers are of paleontological relevance because they are mostly composed of larger foraminifera accumulations, playing a lithogenetic role. The first layer is predominantly composed of large agamonts (megalospheric forms) of *N. perforatus* and much smaller ones of *N. striatus* (Bruguière, 1792), partly comparable to the "nummulite banks" proposed by Arni (1965). At around 37 m, a similar accumulation is visible, but now with large agamonts of *Assilina exponens* (Sowerby, 1840), and lastly, from meter 40 to 44, thick beds of dominant discocyclinids. The lithological description of the succession and additional field data (i.e., ichnofabrics, gamma-ray emission, and the fossil content) are summarized in Figs. 2, 3, 4, and Table 1, and the microfacies distribution is illustrated in Fig. 5.

Ichnofabrics of the Capo Mortola section

Six ichnofabric (IF) classes were distinguished and named based on the dominant features and traces in the Capo Mortola section (Figs. 2, 4).

Planolites IF is only recorded in the Cretaceous Trucco Formation (Fig. 2) and is characterized by

Fig. 1 - Location and studied area. A) Map of Italy showing the Liguria region. B) Location map showing Capo Mortola and the studied section. C) Detailed geological map of Capo Mortola, showing the studied section, modified from Dallagiovanna et al. (2012b). D) Lithostratigraphic column of the Provençal Domain, modified from Decarlis et al. (2014). E) Panoramic view of the Capo Mortola outcrop showing the lower part of the Capo Mortola Calcarenite. F) View of the unconformity between the Upper Cretaceous Trucco Formation (K) and the Bartonian Capo Mortola Calcarenite (Ba). G) Detail of the unconformity showing the lithologic change between the Trucco Formation and the Capo Mortola Calcarenite. H) Panoramic view of the intermediate part of the outcrop, corresponding to the Capo Mortola Calcarenite.

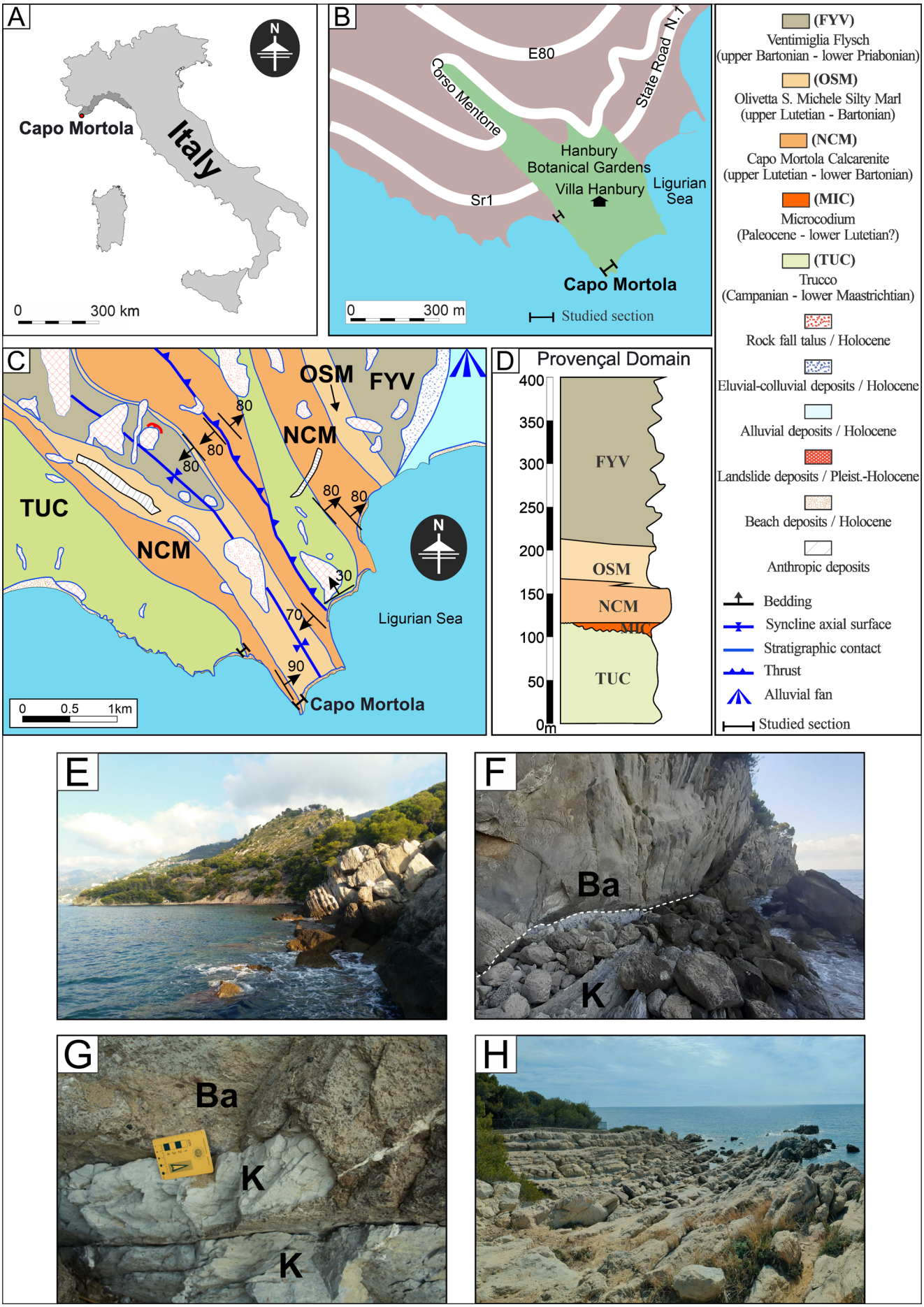
A
Capo Mortola
Italy
N
0 300 km
B
E80
State Road N.1
Corso Mentone
Hanbury Botanical Gardens
Villa Hanbury
Ligurian Sea
Sr1
Capo Mortola
0 300 m
Studied section
C
OSM
FYV
NCM
TUC
NCM
80
80
80
80
80
30
70
90
Ligurian Sea
Capo Mortola
0 0.5 1km
D
Provençal Domain
400
350
300
250
200
150
100
50
0m
FYV
OSM
NCM
TUC
(FYV)
Ventimiglia Flysch
(upper Bartonian - lower Priabonian)
(OSM)
Olivetta S. Michele Silty Marl
(upper Lutetian - Bartonian)
(NCM)
Capo Mortola Calcarenite
(upper Lutetian - lower Bartonian)
(MIC)
Microcodium
(Paleocene - lower Lutetian?)
(TUC)
Trucco
(Campanian - lower Maastrichtian)
Rock fall talus / Holocene
Eluvial-colluvial deposits / Holocene
Alluvial deposits / Holocene
Landslide deposits / Pleist.-Holocene
Beach deposits / Holocene
Anthropic deposits
Bedding
Syncline axial surface
Stratigraphic contact
Thrust
Alluvial fan
Studied section
E
F
Ba
K
G
Ba
K
K
H

Figure 1

Tab. 1 - Lithological description of the Capo Mortola section showing the fossil content recorded in the outcrop.

CAPO MORTOLA					
Stage	**Formation**	**Thickness (m)**		**Lithology**	**Description and fossil content**
Bartonian	**Capo Mortola Calcarenite**	49.34	2.07	Biocalcarenite	Common orthophragminids and rare *Assilina*. Small *Operculina* are recorded abundantly, especially in the middle portion of this bed. Orthophragmines are much smaller and are rare to sporadic toward the top of the bed.
		47.27	0.85		
		46.42	1.78		
		44.64	1.24	Biocalcirudite	Abundant orthophragmines, *Assilina,* and *Nummipera.*
		43.4	2.30		
		41.1	1.3		
		39.8	0.7	Biocalcisiltite	Abundant large B forms of orthophragmines and common *Assilina* and *Nummipera.*
		39.1	1.45	Calcisiltite	Only meniscate burrows are observed.
		37.65	0.26	Biocalcirudite	Grain size increase, and dominant *Assilina* with common *Nummulites.*
		37.39	0.27	Biocalcisiltite	Similar lithology as below, but abundant *Nummulites.*
		37.12	0.18	Calcisiltite	Fining upwards up to a fine silt. There is no recorded fossil content.
		36.94	0.19		
		36.75	1.7		
		35.05	0.82	Biocalcarenite	Abundant corals, bivalves (including oysters), *Nummulites,* and orthophragmines.
		34.23	1.20	Calcisiltite	Barren of fossils.
		33.03	1.2	Biocalcarenite	Abundant *Nummulites* and common corals, and bivalves.
		31.83	1.1	Biocalcirudite	Evidence of bioturbation. The fossil content is characterized by oysters recorded at the base, and corals, echinoids, and *Nummulites* are observed at the top of these beds.
		30.73	1.5		
		29.23	0.35	Biocalcisiltite	Abundant *Nummulites.*
		28.88	0.44	Biocalcirudite	The base is characterized by small *Nummulites* , corals, bivalves, and gastropods. Oysters follow in the middle section of the layer; toward the top, oysters, corals, and N*ummulites* are common. At the top of the layer, abundant *Nummulites* only are recorded.
		28.44	1.96		
		26.48	0.5		
		25.98	0.68		
		25.3	0.8		
		24.5	1.55	Biocalcirudite	Abundant oysters, small bivalves, scaphopods, turritelids, and rare corals are recorded, whereas *Nummulites* (A and B forms) are always present.
		22.95	1.24		Solitary corals and *Nummulites* throughout the entire bed. At 0.50 m from the base, there is an oyster rich horizon.
		21.71	1.8	Biocalcarenite	Coarsening upward with abundant quartz. Abundant mollusks, especially oysters, corals, and *Nummulites* .
		19.91	3.75	Biocalcirudite	*Nummulites* A/B ratio decrease toward the top of the bed; abundant oysters.
		16.16	1.05	Biocalcisiltite	This layer is characterized by a fine-grained matrix with oysters and bivalves.
		15.11	2.92	Biocalcirudite	Occurrences of large flat *Nummulites* and abundant bioturbation.
		12.19	2.15	Biocalcarenite	Abundant *Nummulites* (large and flat) and evidence of bioturbation is visible. At the base of this layer, solitary corals and echinoids are observed.
		10.04	1.86	Biocalcirudite	The upper part of this layer is distinguished by an abundance of small *Nummulites* and common regular and irregular echinoids. Mollusks such as gastropods (turritellids) and bivalves (cardiids, pectinids, oysters), solitary corals, bryozoans, and cylindrical burrows are present.
		8.18	0.40	Biocalcarenite	A reduction in grain size is recorded (fine sand). This layer is characterized by abundant small *Nummulites.*
		7.78	1.54	Biocalcirudite	At the base of this layer, a fine matrix is recorded, becoming coarser towards the top. Abundant *Nummulites.*
		6.24	0.57	Biocalcarenite	A decrease in grain size is recorded (fine sand) with respect to the previous layers. Small *Nummulites* are observed.
		5.67	1.08	Biocalcirudite	The matrix becomes finer-graded toward the top of the layer. At the base, the *Nummulites* A/B ratio is very low.
		4.59	0.78		Fining upward. *Nummulites* (A-forms) are observed at the base of this layer; they disappear toward the top.
		3.81	0.41		Fining upward (fine to medium sand). *Nummulites* A/B ratio decreases toward the top, where B-forms only are preserved (top 0.25 m). Presence of cylindrical burrows.
		3.4	0.56	Biocalcirudite	Includes a conglomerate lens (clast supported) characterized by flint clasts that range between 0.5 cm and 18 cm and coal fragments. *Nummulites* are recorded.
Santonian	**Trucco**	2.84 0	2.84	Marly limestone	Dark-to-dark-grey marl and marly limestones with globotruncanids.

rare horizontal unlined burrows with an infill darker than the surrounding matrix (*Planolites beverleyensis* Billings, 1862). The burrows are ~8 mm in diameter and are superimposed on a massive background sediment consisting of marly limestone. At the sample scale, bioturbation intensity is homogeneously distributed (bioturbation intensity > 70%).

Interpretation: The *Planolites* IF in the Capo Mortola Section is interpreted to represent the work of a deposit-feeding community that colonized a low-hydrodynamic habitat. This interpretation is based on the ethological significance of *Planolites*, which is considered a deposit-feeding burrow (Pemberton & Frey 1982). The intense bioturbation in-

dicates that the sedimentation rate was low enough to cause significant biogenic reworking of the host sediment.

Gastrochaenolites IF (Figs. 2, 4) consists of passively filled hemispherical borings, which are associated with a surface separating the Cretaceous and the Eocene deposits. The borings are preserved as hyporeliefs at the base of a biocalcirudite layer.

Interpretation: The *Gastrochaenolites* IF of the Capo Mortola section represents the work of a filter-feeding community of bivalves that colonized a shallow (foreshore-shoreface) firmground or hardground. *Gastrochaenolites* has been attributed to the activity of bioeroding bivalves (Donovan 2013; Casoli et al. 2016). Present-day producers of *Gastrochaenolites* typically live between the intertidal zone and 25 m depth (Colletti et al. 2020) but are also reported from deeper settings (Bassi et al. 2019). *Gastrochaenolites* is associated with hardgrounds, shellgrounds, and firmground substrates (Donovan, 2003, 2013; Mikuláš & Žítt 2003; Žítt & Mikuláš 2006). The studied specimens of *Gastrochaenolites* are characterized by hemispherical depressions, whereas completely preserved *Gastrochaenolites* appear as clavate borings (Donovan & Hensley 2006; Donovan 2013). This indicates truncation by physical and/or biological erosion (Domènech et al. 2001; Bernardini et al. 2022).

Unlined burrows IF is dominated by horizontal, unlined burrows that are filled with the same material as the host rock (diameter: 3-15 mm). Rare specimens of *Nummipera eocenica* Hölder, 1989 are also documented. Bioturbation intensity is high (> 90%) and homogeneously distributed at the sample scale. Burrowed horizons alternate with metrical horizons with few distinct traces (massive horizons).

Interpretation: The unlined burrows IF in the Capo Mortola section reflects the activity of a benthic community colonizing an offshore habitat characterized by a relatively low sedimentation rate. This interpretation rests on the high bioturbation intensity, indicating that the sedimentation rate was low enough to allow intense biogenic reworking.

Horizontal armored burrows IF is dominated by horizontal burrows that are lined (armored) with foraminiferal tests.

Interpretation: Open nomenclature is used to name the burrows because they are only partially comparable to *Ereipichnus pickerillensis* Ali et al. 2021, which instead is armored with bivalve shells (Ali et al. 2021). They share a foraminiferal lining with *Nummipera*, which is however vertical to oblique (Mendoza-Rodríguez et al. 2020). Armored burrows are often associated with low-energy settings, as shown by *Diopatrichnus*-like burrows in modern sheltered mudflats (Baucon 2021; Baucon et al. 2021), Eocene *Nummipera* in low-energy ramp settings (Jach et al. 2012; Mendoza-Rodríguez et al. 2020), and Pliocene *Ereipichnus* in moderate-energy shoreface environments (Ali et al. 2021).

Teichichnus IF comprises arcuate, retrusive spreite burrows with stacked laminae (*Teichichnus rectus*, Seilacher, 1955; diameter: ~3 cm). *Teichichnus* occurs in mono-ichnospecific assemblages, and it is superimposed on a massive background sediment in the upper part of the Capo Mortola Calcarenite (Figs. 2, 4).

Interpretation: This IF is interpreted to reflect a community of suspension feeders colonizing a stressed marginal-marine environment influenced by deltaic deposition. This interpretation is based on the typical environmental setting of *Teichichnus rectus*, which occurs in mono-ichnospecific associations in marginal-marine environments with stressed conditions (bays, lagoons, estuaries, or deltas). *Teichichnus* is often reported in salinity-stressed and/or deltaic settings (Knaust 2018).

Nummipera IF is dominated by *Nummipera eocenica*, consisting of vertical to oblique burrows with a wall made of LBF. *Nummipera eocenica* is superimposed to an intensely bioturbated background (bioturbated area >80%). The *Nummipera* IF occurs in the upper part of the Capo Mortola Calcarenite (Figs. 2, 4). Bioturbation intensity is 6- homogeneous at the sample scale.

Interpretation: This ichnofabric represents the work of a benthic community colonizing an offshore habitat with slow sedimentation and well-oxygenated conditions. These physicochemical conditions are suggested by the intense degree of bioturbation and its homogeneous distribution (Taylor et al. 2003; Gingras et al. 2011; Uchman & Wetzel 2011). The interpretation is supported by the known occurrences of *Nummipera eocenica*, which are mostly related to low-energy carbonate middle to distal ramp settings (Jach et al. 2012; Mendoza-Rodríguez et al. 2020).

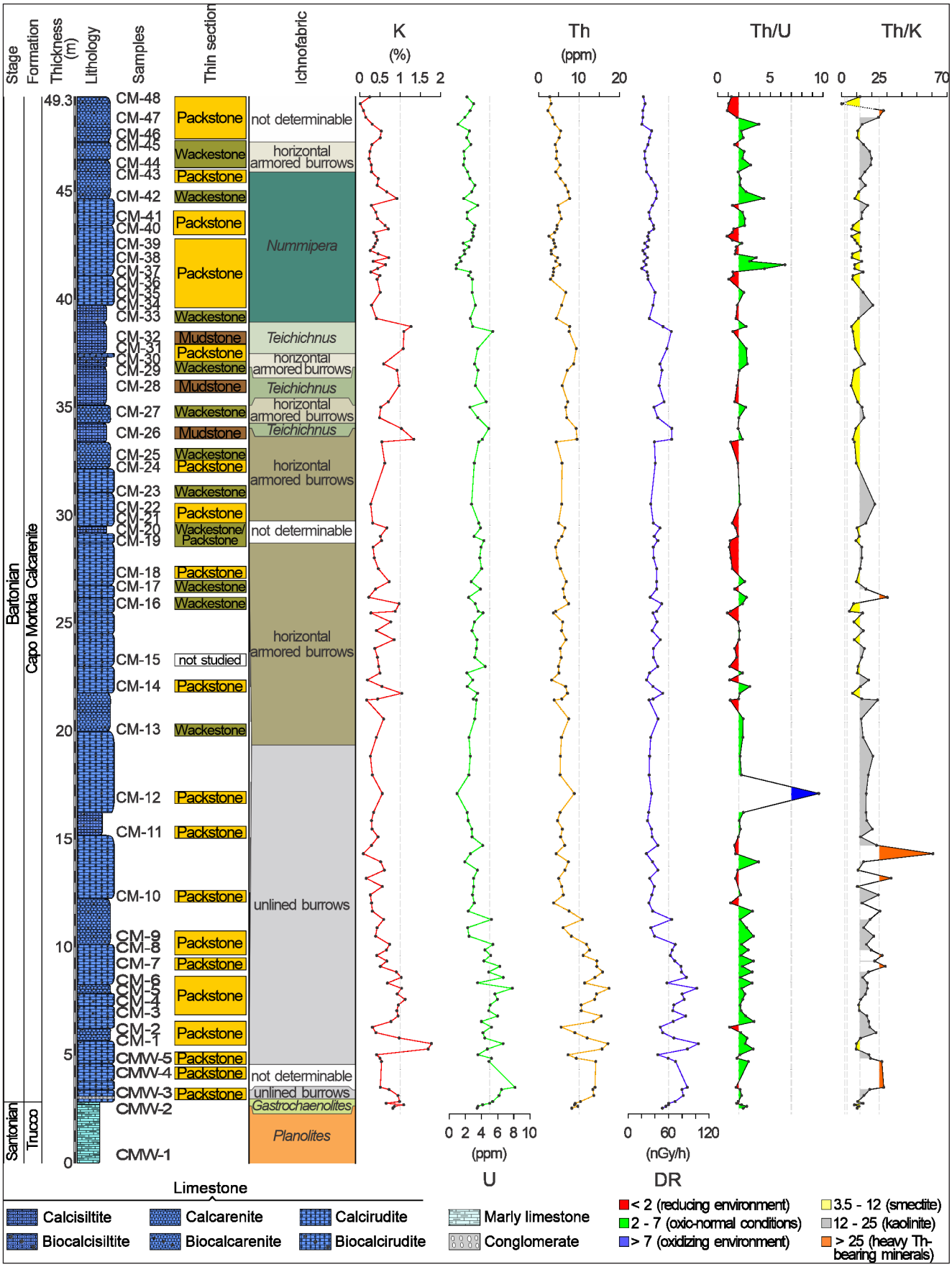

Fig. 2 - Stratigraphic column of the Capo Mortola section displaying the lithological changes, ichnofabrics, and natural gamma ray spectra showing the curves of potassium (K), uranium (U), thorium (Th), dose rate (DR), and the calculated Th/U and Th/K ratios.

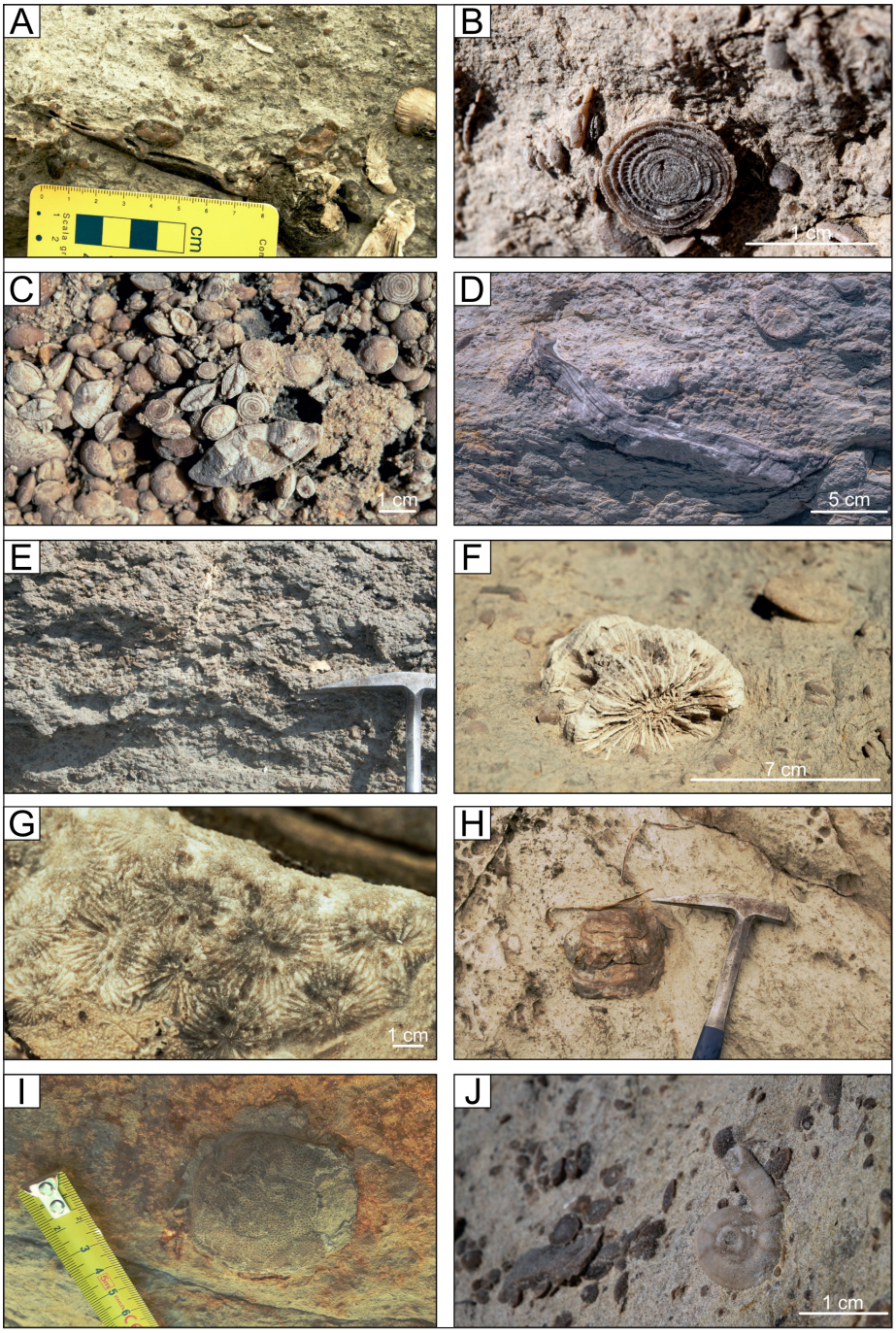

Fig. 3 - Fossil content recorded in the Capo Mortola section. A) Assemblages of *Nummulites* and coral. B) View of a B-form of *Nummulites* (*N. striatus*). C) Close-up showing abundant and diverse forms of *Nummulites*. D) Solitary coral (Scleractinia) and oyster bed. E) Nummulite bank displaying A and B forms near base of section (16.0 m). F) Fragment of a solitary coral (Scleractinia). G) Coral colonies recognized on the surface. H) Outer surface of an oyster valve. I) Dorsal view of a crab carapace. J) Calcareous tube of the serpulid worm *Rotularia spirulaea* (Lamarck, 1818).

Spectral gamma ray

Gamma-ray emissions are higher at the base than at the top of the section (Fig. 2). K (%) concentrations record values between 0.0 and 1.77%, with most of values below 1%. Values above 1% are only observed in some biocalcirudites and biocalcarenites at the base (between 5.26 and 5.51 m; 7.56 m, 8.07 m, and 8.58 m; MF1) and in calcisiltites (between 33.50 and 34.00 m and between 37.7 m and 38.73 m) in the upper part of the section. The concentration of U varies between 0.82 and 8.11 ppm. Most values of U are below 4 ppm almost throughout the section (from MF2 to MF6), except at the base of the succession, where U concentrations are >4.0 ppm (MF1). The Th concentration varies between 2.20 and 17.35 ppm; values below 10 ppm are recorded throughout most of the stratigraphical succession (from MF2 to MF6), except for some samples at the base of the Capo Mortola Calcarenite (biocalcirudite and biocalcarenite; from 2.69 m to 10.11 m; MF1 and base of MF2) that display a significant higher increase in the concentration of Th (>10 ppm). The overall dose rate (DR) varies from 19.48 to 103.36 nGy/h. For most of the

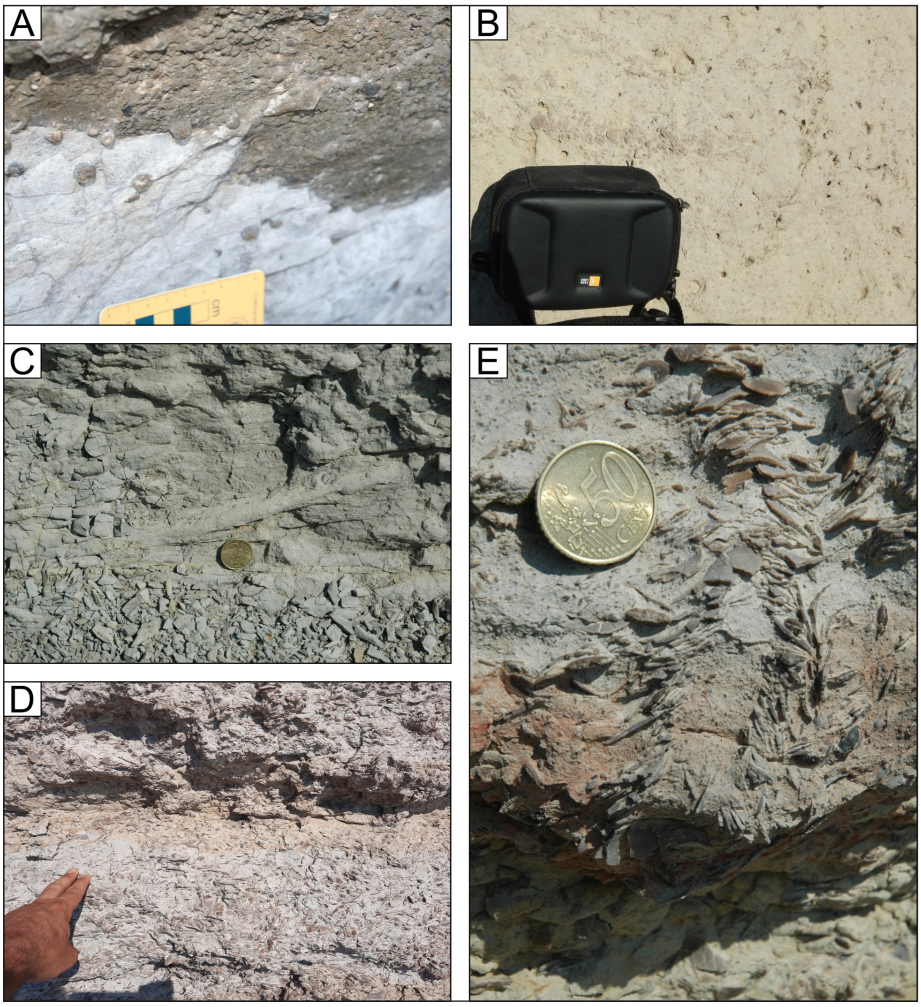

Fig. 4 - Ichnofabrics recorded in the Capo Mortola section. A) *Gastrochaenolites* IF exposed at the boundary between the Cretaceous and the Eocene deposits with several passively filled hemispherical borings (*Gastrochaenolites*). B) Horizontal armored burrows IF. At the center of the image is an individual specimen of a horizontal burrow lined with foraminiferan tests. C) *Teichichnus* IF. A spreite burrow characterized by stacked laminae (*Teichichnus rectus*) is documented. D) *Nummipera* IF. E) *Nummipera* IF showing a vertical burrow (*Nummipera*) with a wall consisting of larger benthic foraminifera.

section, DR are lower than 60 nGy/h (mean 34.04 nGy/h) except for the base of the succession (from 2.69 m to 10.11 m; MF1 and base of MF2) and the upper part of the section (between 33.50 and 34.00 m and between 37.7 m and 38.73 m; MF5), where DR values are higher than 60 nGy/h (a mean of 71.67 nGy/h). The Th/U ratio ranges from 0.84 to 9.60 with most values throughout the section being comprised between 2 and 7 and with values located at the base of the Capo Mortola Calcarenite (biocalcirudite and biocalcarenite; from 2.69 m to 10.11 m; MF1 and base of MF2). Values of the Th/U ratio <2 are also common throughout the section, especially in the middle and upper parts (from MF3 to MF6). A value of the Th/U ratio >7 is only observed in the biocalcirudite located at 17.12 m from the base of the section (MF2). The Th/K ratio fluctuates between 0 and 60.57 with most values being comprised between 12 and 25, especially at the base and in the middle part of the succession (MF1, MF2, and MF3), and corresponding to the various lithologies. Th/K ratios values comprised between 3.5 and 12 also occur the section and dominate in its upper part (from MF3 to MF6). Th/K ratios >25 are rarely recorded at the base (3.50 m, 4.69 m, 9.09 m, 9.60 m, 13.18 m, and 14.33 m; MF1, MF2, and MF3) and at the top (48.60 m; MF4) of the studied section.

Fig. 5 - Cluster analysis based on Ward's method and photomicrographs of thin sections from the Capo Mortola section with their corresponding microfacies. Photomicrographs: A) Microfacies MF1: packstone (CM6; 8.50 m). B) Microfacies MF1: packstone (CM6; 8.50 m). C) Microfacies MF1: packstone (CM6; 8.50 m). D) Microfacies MF2: packstone (CM11; 15.25 m). E) Microfacies MF2: packstone (CM11; 15.25 m). F) Microfacies MF3: packstone (CM31; 37.40 m); G) Microfacies MF3: packstone (CM24; 32.18 m). H) Microfacies MF4: packstone (CM48; 49.20 m). I) Microfacies MF5: mudstone (CM28; 36.0 m). J) Microfacies MF6: packstone (CM36; 40.80 m). K) Microfacies MF6: packstone (CM34; 39.70 m). Di = *Ditrupa*; Or = *Orbitolites*; Orph = ortophragmines; As = *Assilina*; Nu = *Nummulites*; Pf = planktonic foraminifera.

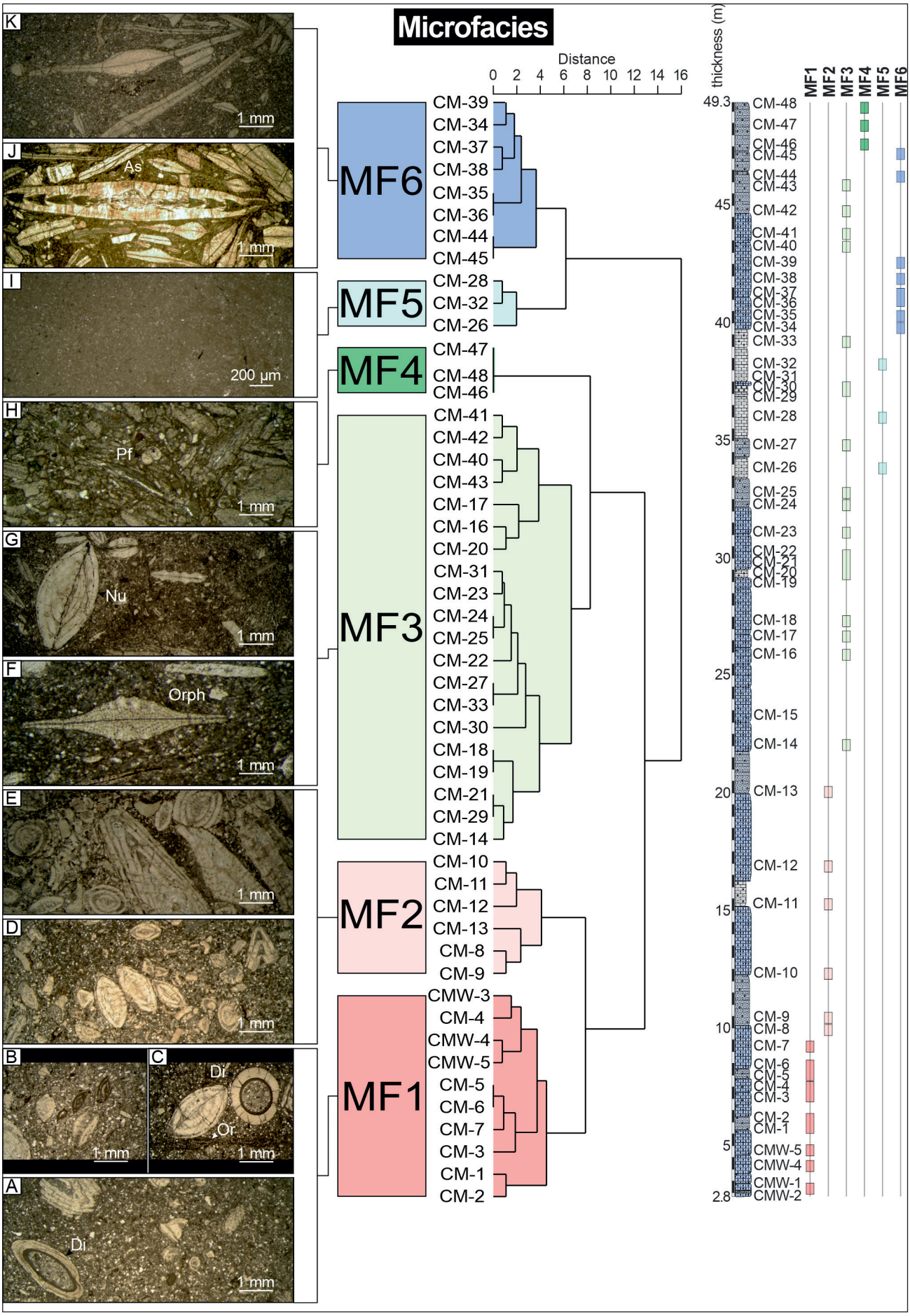
Microfacies
Distance
0 2 4 6 8 10 12 14 16
thickness (m)
MF1 MF2 MF3 MF4 MF5 MF6
MF6
MF5
MF4
MF3
MF2
MF1
CM-39 CM-34 CM-37 CM-38 CM-35 CM-36 CM-44 CM-45
CM-28 CM-32 CM-26
CM-47 CM-48 CM-46
CM-41 CM-42 CM-40 CM-43 CM-17 CM-16 CM-20 CM-31 CM-23 CM-24 CM-25 CM-22 CM-27 CM-33 CM-30 CM-18 CM-19 CM-21 CM-29 CM-14
CM-10 CM-11 CM-12 CM-13 CM-8 CM-9
CMW-3 CM-4 CMW-4 CMW-5 CM-5 CM-6 CM-7 CM-3 CM-1 CM-2
49.3 CM-48 CM-47 CM-46 CM-45 CM-44 CM-43 45 CM-42 CM-41 CM-40 CM-39 CM-38 CM-37 CM-36 CM-35 40 CM-34 CM-33 CM-32 CM-31 CM-30 CM-29 CM-28 35 CM-27 CM-26 CM-25 CM-24 CM-23 CM-22 30 CM-21 CM-20 CM-19 CM-18 CM-17 CM-16 25 CM-15 CM-14 20 CM-13 CM-12 CM-11 15 CM-10 CM-9 10 CM-8 CM-7 CM-6 CM-5 CM-4 CM-3 CM-2 CM-1 5 CMW-5 CMW-4 CMW-1 2.8 CMW-2
K 1 mm
J As 1 mm
I 200 µm
H Pf 1 mm
G Nu 1 mm
F Orph 1 mm
E 1 mm
D 1 mm
B 1 mm
C Di Or 1 mm
A Di 1 mm

Figure 5

Microfacies analysis

Six different microfacies were recognized in the Capo Mortola section; Pearson's correlation coefficient calculated for microfacies is 0.7863, indicating significant clustering within the studied data (Fig. 5):

Microfacies MF1 corresponds to a packstone that occurs at the base of the Capo Mortola section (from samples CMW-3 to CM-7), which records poorly to moderately sorted grains larger than 2 mm with rare LBF, especially nummulitids, smaller benthic foraminifera (SBF), serpulids (*Ditrupa*), and mollusks. The remaining samples of this microfacies are composed of an unsorted packstone with carbonate components made up of different and abundant *Nummulites* (*N. perforatus*, *N. brongniarti* (d'Archiac & Haime, 1853) and *N. puigsecensis* Reguant & Clavell, 1967), *Orbitolites complanatus* (Lamarck, 1801), planktonic foraminifera (PF), SBF, abundant serpulids (*Ditrupa*), rare corals, and mollusks. The siliciclastic components are medium- to coarse-sized quartz grains. The matrix is composed of silt and fine sand, with rare glauconite grains.

Microfacies MF2 (from sample CM-8 to CM-11) is an unsorted packstone with an increase in the biotic component compared to MF1, mainly consisting of two dominant species of *Nummulites* (*N. perforatus* and *N. puigsecensis*), rare *Assilina exponens*, SBF, PF, mollusks, corals, and serpulids (*Ditrupa*). The main non carbonate components are: medium-sized quartz and glauconite grains, organic matter scattered in a matrix made of clay and silt.

Microfacies MF3 is a mix of unsorted wackestone and packstone with varying biotic content, such as *Nummulites beaumonti* d'Archiac & Haime, 1853 and *N. biarritzensis* d'Archiac in Bellardi, 1852, *Assilina exponens,* small (< 1 cm) orthophragmines, *Asterigerina,* SBF (mostly small rotaliids), PF, mollusks, rare echinoderms, serpulids (*Ditrupa*), calcareous red algae, and coral fragments (colonial). The matrix is made up of clay and silt (50-70%), in which some glauconite grains are scattered and organic matter is recorded.

Microfacies MF4 is an unsorted packstone; in contrast to the microfacies described above, the matrix made up of clay and silt is less than 30%. The biotic content is very abundant, including orthophragmines, *Nummulites* spp., abundant small-sized (< 1 cm) *Operculina* sp., SBF (small rotaliids), abundant PF, mollusks, rare echinoderms, and serpulids (*Ditrupa*). Glauconite grains and scattered organic matter occur in some samples of this microfacies.

Microfacies MF5 is a mudstone with scarce biotic content (SBF, PF, and rare mollusks). Well-rounded quartz grains and glauconite grains are observed.

Microfacies MF6 is a well-sorted wackestone and packstone characterized by a matrix (between 70% and 90%) made up of clay and silt; the siliciclastic component is composed of medium- to coarse-sized quartz grains. Rare glauconite grains are recorded in most samples of this microfacies, except in samples CM44 and CM45, where a higher abundance is documented. Scattered organic matter is observed. The biotic content is characterized by abundant orthophragmines (groups of *Discocyclina dispansa*, *D. pulchra* (Checchia-Rispoli, 1909), and *D. pratti* (Sowerby, 1846)) and rare *Nummulites* spp. (almost exclusively *N. biarritzensis*), *Operculina* sp., *Asterigerina*, SBF, PF, mollusks, rare echinoderms, and serpulids (*Ditrupa*).

Discussion

Spectral gamma ray and paleoclimate

The higher values of K, U, and Th found in the calcirudite and calcarenite at the base of the Capo Mortola section (between 2.54 m and 8.83 m; Fig. 2) must be interpreted with caution due to the possibility that these concentrations are not related to the pristine rock signal but are rather a modern disequilibrium of these elements as they are constantly washed by swells and waves that intensively corrode the surfaces of the rocks and sporadically reach deep inside the layers (Fig. 1G). This disequilibrium, especially in U and Th, is known to occur when the outcrop is exposed to groundwater or seawater (e.g., Cassidy 1981; Bessa 1995; Bessa & Hesselbo 1997).

The Th/U ratio, in the remainder of the studied section, stays within the range related to normal marine conditions (Th/U ratio: values from 2 to 7); some samples are characteristic of a reducing environment (Th/U ratio: values less than 2); and one peak (17.12 m; calcirudite) exceeds the upper limit of marine sediments (Th/U ratio: values >7), with a value suggesting oxidizing terrestrial settings (e.g., Schnyder et al. 2006; Kouamelan et al. 2020) (Figs. 2 and 6A). This single peak seems rather unrealistic and can probably be linked to either a local anomaly or a measuring error; it can be discarded.

The Th/K ratio is used to identify clay minerals (illite, chlorite, montmorillonite, and kaolinite), micas, glauconite, and K-feldspars. The Th/K ratio depends on the nature of the clay mineral assemblages, which in turn is controlled by climate (e.g., Quirein et al. 1982; Bessa 1995; Fabricius et al. 2003; Kouamelan et al. 2020). Lithology, depositional environment, and paleoclimate all exert significant control over clay mineral genesis (Ruffell & Worden 2000; Gao et al. 2018; Kouamelan et al. 2020). Clay minerals (chlorite, glauconite, illite, kaolinite, and smectite), which have different Th/K ratio values, have been interpreted through Schlumberger´s (1997) crossplot: high Th/K ratios (from 12 to 25) are associated with abundance of kaolinite, intermediate Th/K ratios (from 3.5 to 12) are related to montmorillonite (smectite), low Th/K ratios (from 2.0 to 3.5) are linked with illite, and heavy thorium-bearing minerals display Th/K ratios greater than 25 (e.g., Schlumberger 1997; Figs. 2 and 6B).

The good correlation between the Th/K ratio determined from spectral gamma-ray indicates palaeoclimatically significant variations in clay ratios. These changes in the clay concentrations have been compared with studies derived from XRD and XRF, which yield similar results, suggesting that the variation of Th and K is reflected in a determinate clay mineral, showing a common control on their variation (Ruffell & Worden 2000; Deconinck et al. 2003; Schnyder et al. 2006; Hesselbo et al. 2009). For this reason, the Th/K and Th/U ratios are climate sensitive indicators that, supported by the responses of other proxies, provide a primary paleoclimatic interpretation.

The Th/K crossplot identified montmorillonite, sourced from smectite, and kaolinite as the dominant clay minerals, whereas heavy thorium-bearing minerals are recorded as traces in the Capo Mortola section (Figs. 2 and 6B). These clay mineral assemblages, reflected in the Th/K ratio, are controlled by climatic variations (Bessa 1995; Kouamelan et al. 2020). The genesis of smectite (montmorillonite) is attributed to the chemical weathering of soils in warm to temperate climates with seasonal climate fluctuations associated with humid/arid regimes (e.g., Deconinck 1992; Diester-Haass et al. 1998; Kennedy & Wagner 2011). Kaolinite is associated with tropical soils, characterized by humid climate and well-drained areas, as the result of highly hydrolytic weathering reactions with considerable removal of K from the soil profile (e.g., Robert & Chamley 1991; Bessa 1995; Chamley 2001; Deconinck et al. 2003).

The Capo Mortola section displays an increase in smectite toward the upper portion of the succession, where it alternates with kaolinite, suggesting a probable climatic influence. Whereas kaolinite mostly indicates humid conditions, it is not ruled out that smectite might indicate dry phases (e.g., Bessa 1995; Adatte et al. 2000; Hesselbo et al. 2009). It is reasonable to assume that both kaolinite and smectite are controlled by climatic fluctuations of warm-humid conditions passing to seasonal humid-dry alternations. This climate variation might have caused an alternation between dry and humid conditions that are typically recorded throughout the middle Eocene in the Western Tethys, where the increase in temperature could have altered climate conditions, heightening the hydrological cycle with consequences on the terrigenous supply in the basins (Held & Soden 2006; Chou et al. 2013; Marvel & Bonfils 2013; Baatsen et al. 2020), as seen in comparable geological settings (e.g., Turkey: Rego et al. 2018; Giorgioni et al. 2019. Spain: Peris Cabré et al. 2023. Tunisia: Messaoud et al. 2021. Italy: Spofforth et al. 2010; Gandolfi et al. 2023; Briguglio et al. 2024; Arena et al. 2024; Giraldo-Gómez et al. 2024).

Paleoenvironmental reconstruction

Two different depositional settings are recorded in the Capo Mortola section separated by a regional unconformity recording a gap of at least 25 million years, dividing the Upper Cretaceous deep-water sediments rich in globotruncanids of the Trucco Formation from the middle Eocene shallow-water deposits of the Capo Mortola Calcarenite (Figs. 1G and 2).

The transition from the Cretaceous to the Eocene deposits is characterized by a bioerosional ichnofabric (*Gastrochaenolites* IF) superimposed on a softground ichnofabric (*Planolites* IF) (Fig. 2). Consolidation of the *Planolites*-bearing deposits provided suitable substrates for bioeroding bivalves that produced the *Gastrochaenolites* IF. The *Gastrochaenolites* IF indicates a rocky shore as the substrate for the deposition of the Capo Mortola Calcarenite that was subsequently subject to significant erosion or weathering.

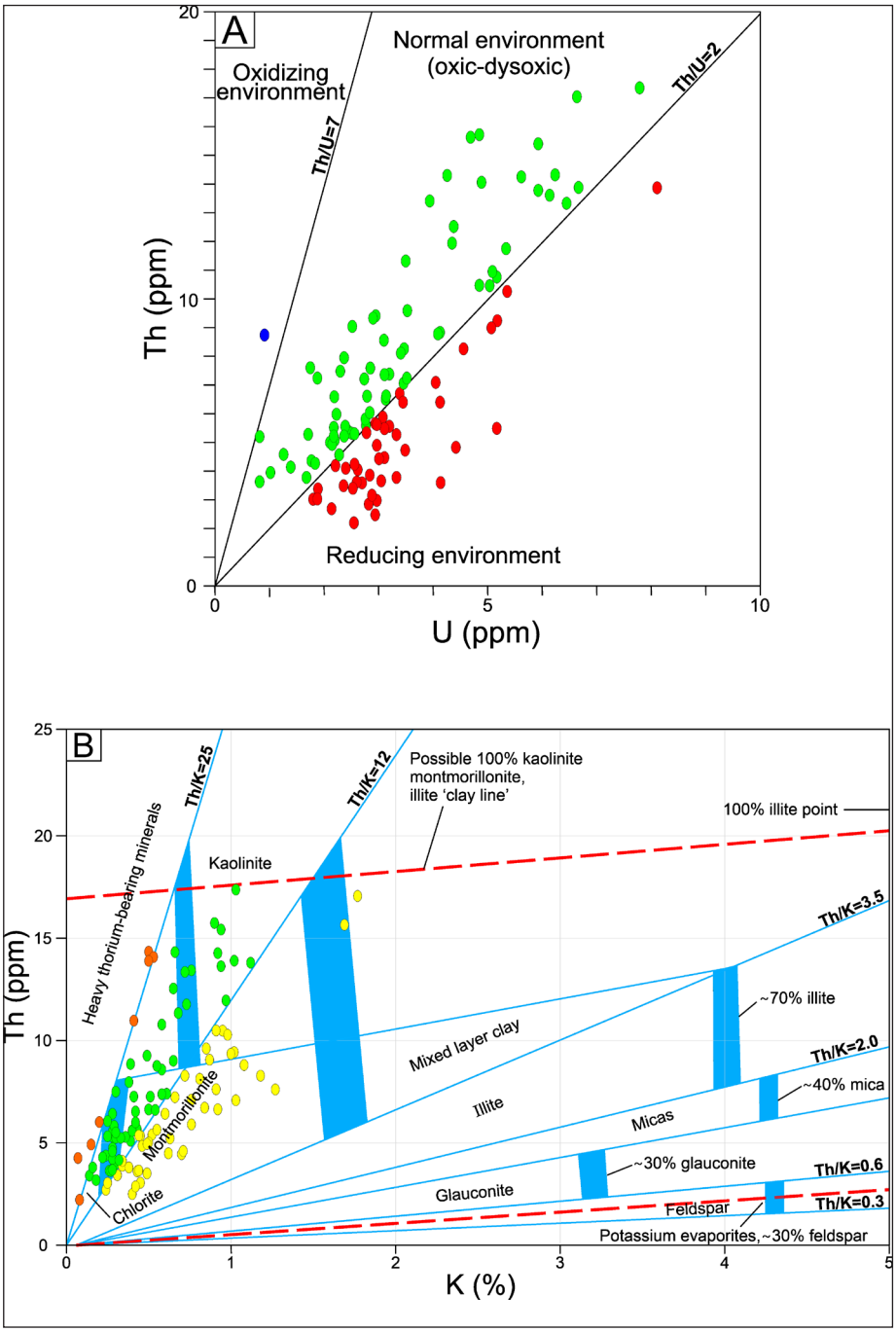

Fig. 6 - Cross-plot analyses of the Th and K. A) Cross-plot of Th/U from samples of the Capo Mortola section showing oxidizing (blue circles), oxic-normal (green circles), and reducing (red circles) environments. B) Cross-plot of Th/K displaying different clay mineral content in the Capo Mortola section based on the Schlumberger (1997) chart: Th/K ratio 3.5–12 (yellow circles): smectite (montmorillonite); Th/K ratio 12–25 (green circles): kaolinite; Th/K ratio >25 (orange circles): heavy thorium-bearing minerals.

The data presented here can represent three different time intervals (Fig. 7), which record the evolution of the carbonate ramp through the middle Eocene (Bartonian). These intervals are derived from a combination of microfacies analysis, fossil content, ichnofabric interpretation, and gamma ray emissions.

Interval I (2.84 – 21.76 m). This interval corresponds to the lower part of the Capo Mortola Calcarenite, which is characterized by microfacies MF1 and MF2 (Figs. 2, 5, and 7). The concentrations of K and Th decrease and the Th/U ratio fluctuates between normal and reducing conditions, indicating probably a terrigenous input within a rather inner distal environment (Figs. 2 and 6A).

The benthic fauna in this interval consists almost exclusively of thick LBF, especially *Nummulites* (mostly *N. perforatus*, followed by *N. puigsecensis*, and rare *N. striatus*), showing a relative abundance of agamonts (i.e., B-forms sensu Hottinger 2006) that may have thrived in relatively calm waters where gametes have higher chances to form the diploid generation (Beavington-Penney & Racey 2004; Bea-

vington-Penney et al. 2006). The relative abundance of B forms might also have permitted the rapid development of low positive reliefs on the seafloor (Seddighi et al. 2015; Briguglio et al. 2017), thus permitting higher chances of preservation of the small A forms as well as gametogenesis keep up agamont production (Kövecsi et al. 2022). The presence of *O. complanatus* at the base of this interval (MF1) indicates a vegetated substrate, as observed in modern environments where Soritinae thrive in waters between 20 and 40 m (Beavington-Penney & Racey 2004; Beavington-Penney et al. 2006; Tomás et al. 2016; Tomassetti et al. 2016; Roslim et al. 2019; Coletti et al. 2021).

Furthermore, the 'unlined burrows' IF indicates that the sedimentation rate was low enough to allow intense biogenic reworking (Bromley 1996). The presence of echinoids, mollusks (gastropods and bivalves), solitary corals, bryozoans, and serpulids (*Ditrupa*) in this interval demonstrates that environmental conditions were favorable for the coexistence of diverse taxa under a shallow-water hydrodynamic regime.

Interval II (21.76 – 39.76 m). This interval corresponds to the intermediate part of the Capo Mortola Calcarenite, which is mainly characterized by MF3, with some intercalations of MF5 in its upper part (Figs. 2, 5, and 7). The lower and middle parts of interval II are dominated by the 'horizontal armored burrows' IF, which alternates in the upper part (35–39 m) of the interval with the *Teichichnus* IF.

The relatively low concentrations of K, U, and Th in MF3 (wackestone and packstone), in contrast to the high values in MF5 (mudstone), are reflected in the lower Th/U ratio, suggesting reducing marine conditions (Koptíková et al. 2010; Kalvoda et al. 2011; Fig. 2). The high values of K, Th, and Th/U ratio in MF5 suggest an increased argillaceous fraction in MF5, coinciding with the lower abundance of LBF and the dominance of SBF and PF. The sedimentary environment is therefore interpreted as slightly deeper than before but still influenced by deltaic contributions. *Teichichnus* has been frequently reported from deltaic paleoenvironments (Buatois et al. 2008; Loughlin & Hillier 2010; Knaust 2018), and the low values of K and Th in MF3 support the same hypothesis (e.g., Bessa 1995). The incipient dominance of *Assilina* (best adapted to lower light radiations; Hottinger 1997; Scheibner et al. 2007) over *Nummulites* (which is less abundant at lower irradiation levels) seems consistent as well. Toward MF5, the deltaic system could have been partially responsible for the increase in the argillaceous fraction as well as for the shift toward a SBF-dominated community. In shallow-water settings, at intermediate depths where *Assilina* dominates, a minor shift in riverine activity is immediately revealed by a sudden change in communities of LBF, as they are sensitive to seafloor irradiation, which is reduced with enhanced riverine inputs.

Such microfacies alternation (i.e., MF3 and MF5; Figs. 2, and 5) correlates with the Th/K ratios: MF5 is found with low Th/K ratios, whereas MF3 occurs during intervals with higher Th/K ratios. This can be interpreted as consequence of oscillating deltaic regimes with fluctuating sedimentary input during periods (i.e., with higher Th/K values), in arid/humid seasonal alternations, and oscillations in runoff and water turbidity where alternation of the benthic community is visible. Mixo- to autotrophic organisms such as corals and LBF flourish during warm and arid periods with reduced water turbidity, whereas gastropods, sea urchins, and SBF thrive as soon as conditions get more humid and runoff and water turbidity increase.

On the other hand, under wet/humid climatic conditions (low Th/K ratios), planktonic-rich silty sediments are deposited (i.e., MF5). Deposition during interval II took place in slightly deeper water than that of time interval I, but still under oxygenated conditions and moderately illuminated seafloors. The increasing dominance of *Assilina*, the continuous presence of *Nummulites*, the low abundance of orthophragmines, and the lack of planktonic foraminifera could indicate a seafloor between 40 and 60 m of water depth (Bassi 1998; Beavington-Penney & Racey 2004).

Interval III (39.76 – 49.30 m). This interval corresponds to the upper part of the Capo Mortola Calcarenite, characterized by microfacies MF3, MF4, and MF6 (Figs. 2, 5, and 7), which display a shift marked by an abrupt upward transition to significantly more distal microfacies according to their fossil content. Low concentrations of K and Th, in comparison with interval II, and variations of the Th/U ratio between a normal and reducing environment, suggest a decreasing influence of the terrigenous input (e.g., Bessa 1995) and a deepening of the carbonate ramp.

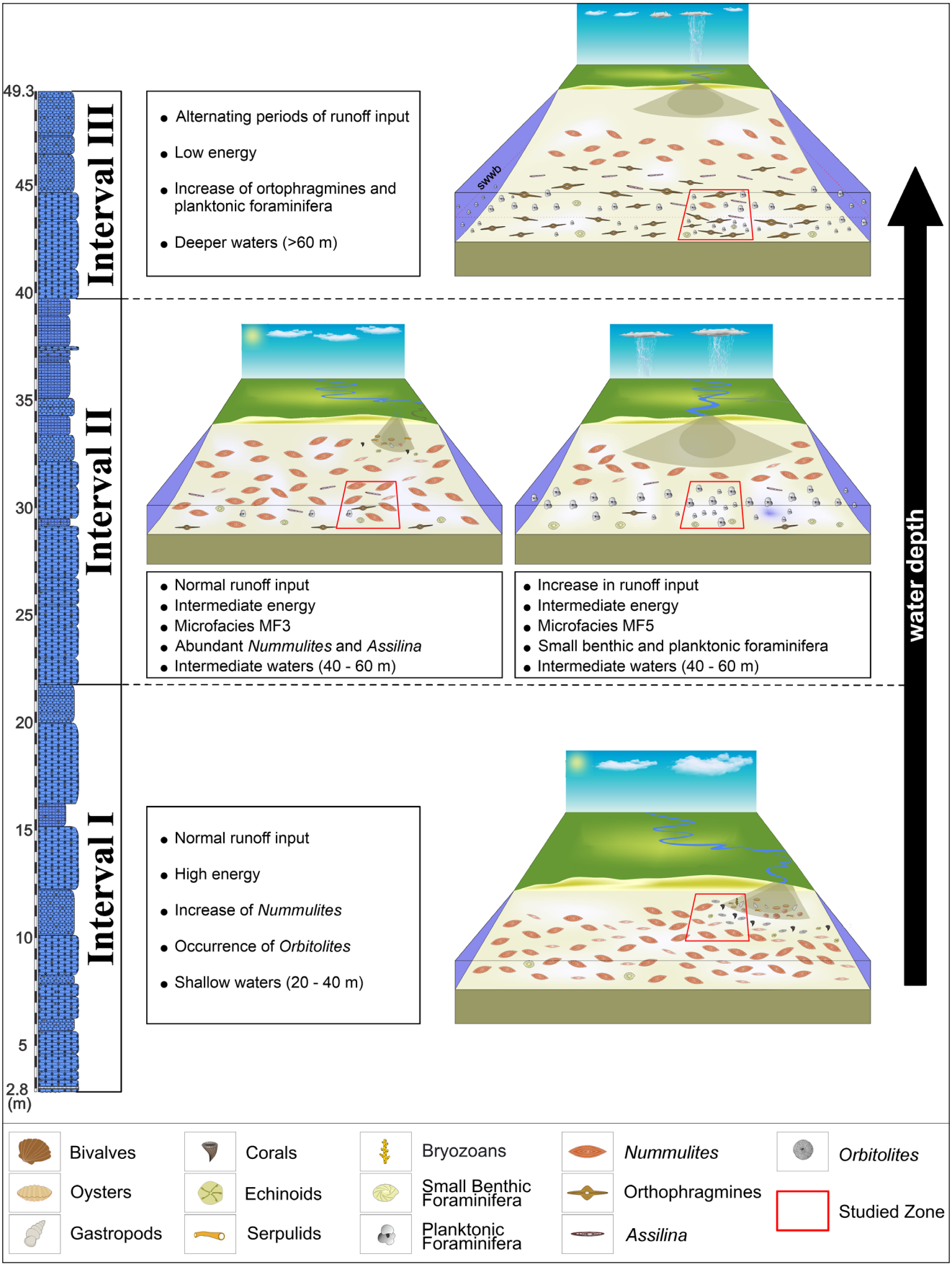

Fig. 7 - Paleoenvironmental evolution of the carbonate ramp at the Capo Mortola section, showing the benthic and planktonic communities at three intervals through the middle Eocene (Bartonian). (Storm weather wave base: swwb).

The Capo Mortola Calcarenite Formation (Nummulitic Limestone)							
Section	**Location**	**Drowning Facies**	**Depositional environment**	**Gravity flows**	**Fossils (transported)**		**References**
					Abundant	**Common**	
Capo Mortola (1)	Maritime Alps Italy	Mudstone to packstone (Calcisiltite to calcirudite)	Middle to outer ramp	No	Planktonic foraminifera, Orthophragmines	*Operculina* benthic foraminifera	This study Brandano 2019 Coletti et al. 2021
Sealza (2)	Maritime Alps Italy	Mudstone to packstone (Calcisiltite to calcirudite)	Middle to outer ramp	No	Planktonic foraminifera, Orthophragmines	*Operculina* benthic foraminifera	Briguglio et al. 2024 Gandolfi et al. 2023
Olivetta SM (3)	Maritime Alps Italy	Mudstone to packstone (Calcisiltite/marl to calcirudite)	Outer ramp	Yes	Planktonic foraminifera, Orthophragmines	Orthophragmines, bivalves, benthic foraminifera	Giraldo-Gómez et al. 2024 Arena et al. 2024 Varrone and Clari 2003
Trucco (4)	Maritime Alps Italy	Mudstone - wackestone (marl and silstone)	Outer ramp	Yes	Planktonic foraminifera, Orthophragmines	*Nummulites,* bivalves, gastropods, echinoderms, corals	Varrone and Clari 2003 Varrone and Decrouez 2007
Croce di Sapalea (5)	Maritime Alps Italy	Mudstone to packstone (Calcisiltite to calcirudite)	Outer ramp	Yes	Planktonic foraminifera, Orthophragmines	*Nummulites,* bivalves, gastropods, echinoderms, corals	Varrone and Clari 2003 Varrone and Decrouez 2007
Roche du Tron (6)	Maritime Alps France	Mudstone to packstone (Calcisiltite to calcirudite)	Outer ramp	Yes	Planktonic foraminifera, Orthophragmines	*Nummulites,* bivalves, gastropods, echinoderms, corals	Varrone and Clari 2003 Varrone and Decrouez 2007
Monte Forquin (7)	Maritime Alps France	Mudstone to packstone (Calcisiltite to calcirudite)	Outer ramp	Yes	Planktonic foraminifera, Orthophragmines	*Nummulites,* bivalves, gastropods, echinoderms, corals	Varrone and Clari 2003 Varrone and Decroues 2007

Tab. 2 - The upper part of the Capo Mortola Calcarenite Formation in the southernmost Provençal Domain (Maritime Alps), showing the lithology and fossil content characteristic in the drowning ramp of different sections during the Bartonian: Capo Mortola (1); Sealza (2); Olivetta San Michele (3); Trucco (4); Croce di Sapalea (5); Roche du Tron (6); and Monte Forquin (7). (The numbers in parentheses of the sections indicate the location on the map in Fig. 10).

The abrupt appearance of the *Nummipera* IF in interval III is interpreted as a product of progressive transgressive conditions, as evidenced by several authors (e.g., Jach et al. 2012; Mendoza-Rodríguez et al. 2020). In the Eocene deposits of the Tatra Mountains (Poland), *Nummipera* is associated with abrupt facies changes during progressive deepening of the carbonate ramp (Jach et al. 2012).

The sudden increase and almost complete dominance of orthophragmines follows the disappearance of the large *Nummulites* and *Assilina*, thus confirming a continuous deepening trend characterized by lower irradiation at the seafloor, which was only colonized by extremely flat LBF with high surface area to volume radio to provide maximum irradiation area for their symbionts (Hohenegger & Briguglio 2012; Molina et al. 2016; Briguglio et al. 2017; Hohenegger et al. 2019). Such flat tests are also in equilibrium with very low hydrodynamic energy, as is typical of deeper seafloors. The abundance of LBF such as ortophragmines and *Operculina* suggests the lowest part of the oligophotic zone, associated with a water depth between 60 and 100 m and below storm weather wave base (Beavington-Penney & Racey 2004; Beavington-Penney et al. 2006; Bassi et al. 2012, 2019; Molina et al. 2016; Briguglio & Rögl 2018; Kövecsi et al. 2022; Arena et al. 2024). This water depth is also corroborated by the increase in the abundance of planktonic foraminifera, as in the Sealza section (Gandolfi et al. 2023), where they have been used to infer a water depth comprised between 60 and 100 m. According to lithology, fossil content, ichnofabric, and spectral gamma ray data, interval III could be related to the relatively rapid sea-level rise in the Bartonian associated with the early stage of drowning of the ramp.

Climate control in the regional configuration of drowning ramps

The Capo Mortola section, given its geodynamic context within the Ligurian Alps in the Provençal Domain, records the incipient formation of a foreland basin initially with the deposition of shallow-water carbonate sediments, followed by deeper-water marly deposits (Sinclair 1997; Giammarino et al. 2010; Perotti et al. 2012; Brandano 2019).

Similar conditions are recognized in several outcrops over a much larger scale, along the modern Maritime Alps, spanning from the Ligurian coast up to the Italy-Switzerland border. All evidence points to a very large ramp that during the middle Eocene underwent significant drowning (Sayer 1995; Sinclair et al. 1988; Allen et al. 2001). The Capo Mortola succession does not record evidence of gravity flows, which are described in almost all successions

in the area (Varrone & Clari 2003; Varrone & Decrouez 2007; Coletti et al. 2021), except at Sealza (Briguglio et al. 2024), which is also the closest one to the Capo Mortola outcrop. Gravity flows are observed in the northernmost sections (Trucco, Olivetta San Michele, Croce di Sapalea, Roche du Tron, Monte Forquin) and are interpreted to have been deposited in an outer ramp setting (Fig. 8; table 2; see references therein), triggered by enhanced deltaic activity and possibly by the tectonic instability of the area. It is therefore possible to add several details to the configuration of the drowning ramps recorded in the Maritime Alps, especially during the early stages of subsidence of the Alpine foreland basins during the Eocene (Sinclair 1997; Perotti et al. 2012).

A cyclicity in carbonate sedimentation, as a response to climate forcing, in connection with changes in sea-level and terrigenous influx might have differentiated the depositional patterns in the different sectors of the ramp during the middle Eocene (Bartonian), especially in the southernmost Provençal Domain (Sinclair et al. 1998; Giraldo-Gómez et al. 2024). Previously, lithological variations among sections and the possible presence of sediment redeposition and gravity flows have been related to local tectonic instabilities, which triggered different sedimentation rates, within the broader geodynamic context of the evolution of the foreland basin (e.g., Sinclair et al. 1998; Varrone & Clari 2003).

Within this scenario, the outcrops of Capo Mortola (this study) and Sealza (Briguglio et al. 2024) may have been located on a ramp sector that was less prone to sediment instability and perhaps recorded initially shallower conditions than other sections in the northern part of the domain where gravity flow deposits are conspicuous and bear reworked material from much shallower sectors (e.g., the Olivetta SM section; Arena et al. 2024; Giraldo-Gómez et al. 2024). Capo Mortola and Sealza, in this view, may represent the sediment sources for the sediment redeposited in deeper sectors of the ramp in the Ligurian areas. Furthermore, it has been suggested that the provenance of the putative source of the Grès d'Annot siliciclastic units, found in the upper part of the underfilled Trinity (sensu Sinclair 1997), had their origin in Corsica, from the Eocene successions (Ravenne et al. 1987; Mueller et al. 2018), thus providing additional clues for future high-resolution paleogeographic reconstructions.

The influence of shifting humid/arid conditions, as recorded by the Th/K ratio in the upper part of the Capo Mortola Calcarenite (as discussed in this study, the Sealza section: Briguglio et al. 2024, and the Olivetta SM section: Giraldo-Gómez et al. 2024. See Fig 8), indicates that the shallow marine conditions were sensitive to sea level changes and sediment input and transport favored by changing hydrogeological cycles during the middle Eocene in the basins of the Western Tethys (Spofforth et al. 2010; Rego et al. 2018; Giorgioni et al. 2019; Messaoud et al. 2021; Peris-Cabré et al. 2023; Gandolfi et al. 2023; Sharma et al. 2024; Briguglio et al. 2024; Arena et al. 2024; Giraldo-Gómez et al. 2024), coinciding with the MECO event in the Sealza section (Gandolfi et al. 2023), the Capo Mortola section (Gandolfi et al. 2024) and the Olivetta SM section (Gandolfi et al. 2025). In the foreland basin of the Provençal Domain, the MECO starts at once with the initial drowning of the carbonate ramp (Fig. 8).

Conclusions

Based on the lithology, fossil content, ichnofabric analysis, and spectral gamma ray data, the Capo Mortola section shows the early-stage development of a drowning carbonate ramp during the middle Eocene (Bartonian), which unconformably overlies the Upper Cretaceous open-marine deposits in the Liguria region (NW Italy). The main outcomes of this study are as follows:

1. Based on microfacies and ichnofabric (IF) analysis, three main intervals are recognized from the base to the top of the Capo Mortola section, showing the evolution of the middle Eocene carbonate ramp. Interval I is interpreted as the shallower part of the carbonate ramp, with an inferred depth of 20-40 m. Interval II suggests a deepening of the carbonate ramp (40-60 m). Interval III suggests a deeper environment with depths greater than 60 m but still within the photic zone.
2. Changes in larger benthic foraminiferal assemblages closely follow this deepening-upward trend, with higher abundance of *Nummulites* in the shallowest interval I, followed by dominant *Assilina* in interval II and lastly by orthophragmines and *Operculina* in the deepest interval III.

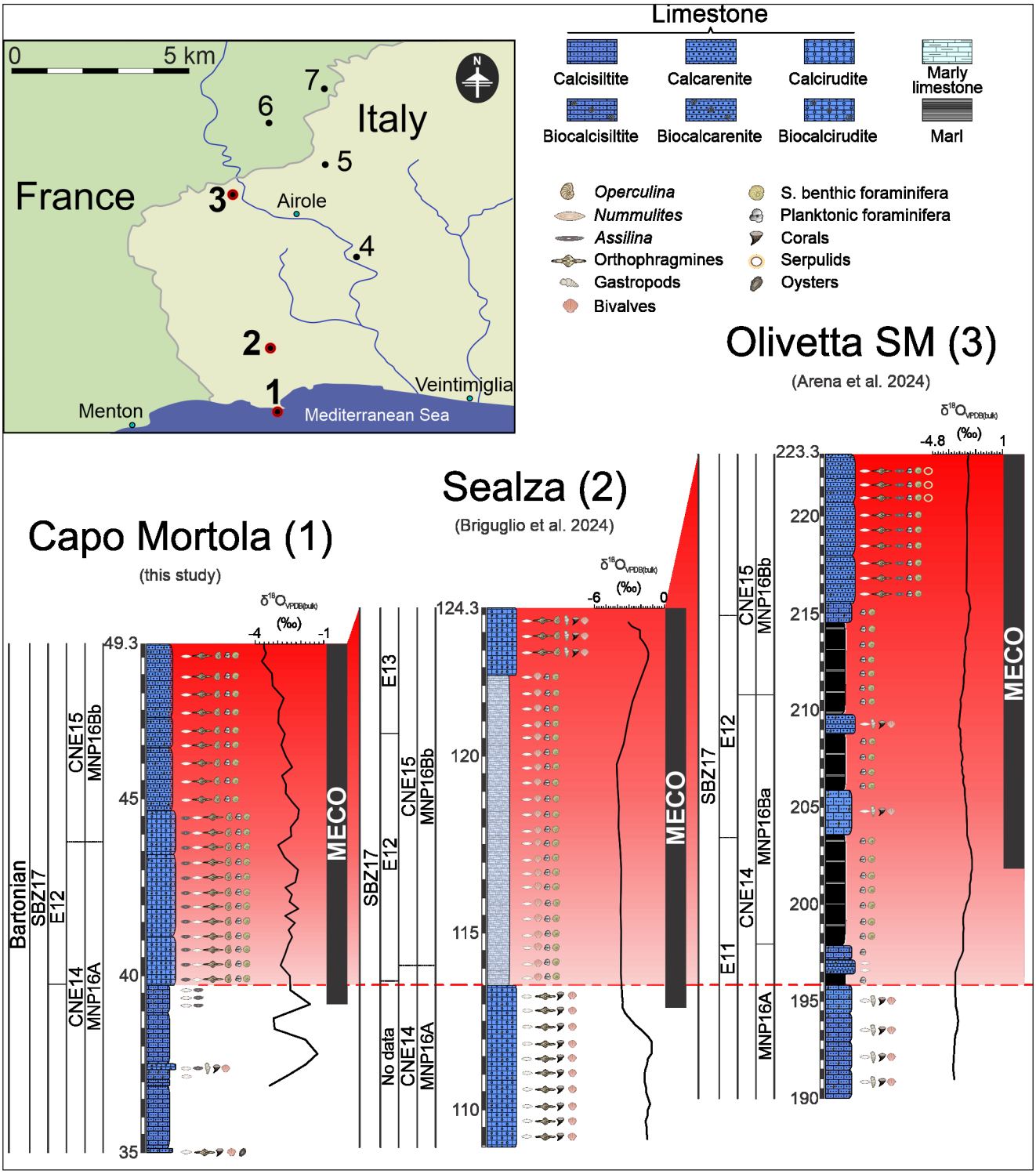

Fig. 8 - The Capo Mortola Calcarenite Formation in the southernmost Provençal Domain (Maritime Alps, France-Italy border). Stratigraphic columns of the upper part of the Capo Mortola Calcarenite Formation of three sections in NW Italy: (1). Capo Mortola section (this study); the position of the Middle Eocene Climatic Optimum (MECO) and biostratigraphy are after Gandolfi et al. (2024). (2). Sealza section (Briguglio et al. 2024); the position of the Middle Eocene Climatic Optimum (MECO) and biostratigraphy are after Gandolfi et al. (2023). (3). Olivetta San Michele section (Arena et al. 2024; Giraldo-Gómez et al. 2024). The map displays the three sections listed above and includes some additional Italian and French sections (Varrone & Clari 2003; Varrone & Decrouez 2007): (4). Trucco section; (5). Croce di Sapalea section; (6). Roche du Tron section; (7). Monte Forquin section. (The red gradient area indicates the increase in abundance of planktonic foraminifera recorded in the three sections).

3. A significant input of terrigenous material from a geographically close fluviatile source is inferred by an increase in the concentration of K and Th, especially in intervals I and II. The variation between normal (oxic - dysoxic) and reducing conditions throughout the entire stratigraphic succession represents a common feature of prodeltaic sediments within deltaic settings. As such, the Capo Mortola succession seems to be much affected by the fluviatile input than all other known sections from the region.
4. In the upper part of the studied Capo Mortola section, fluctuations between a warm-humid climate and a seasonal humid/dry climate happened; those are in accordance with the reconstructed northwestern Tethyan climate during the MECO event

Data Availability Statement

The data supporting the results of this research are available upon request. Interested researchers may contact the corresponding Author to obtain access.

Acknowledgments: This study was supported by the University of Genova, which funded the Curiosity-Driven Project awarded to AB on Ligurian Paleoenvironments, and by the Ministry of Education, University and Research (MIUR), Italy, which funded the PRIN 2017 "Biota resilience to global change: biomineralization of planktic and benthic calcifiers in the past, present, and future" (2017RX9XXY). MP thanks FRA 2024 at the University of Genova for the support of this project. We thank the Hanbury Botanical Gardens Regional Protected Area for sampling permission (permit N° 52863) and for all the logistical help during the last four years of site visits. We thank Wolfgang Eder (formerly at the University of Genova), Sulia Goeting (University of Lausanne), and Eleni Lutaj (University of Genova) for their help in the field.

We thank two anonymous reviewers for their constructive comments, which helped us to improve the manuscript; the editors Proffs. Francesca Bosellini (Unimore), Lucia Angiolini (Unimi) and Fabrizio Berra (Unimi) for their final remarks.

References

Adams J.A. & Weaver C.E. (1958) - Thorium-to-Uranium ratios as indicators of sedimentary processes: Example of concept of geochemical facies. *The American Association of Petroleum Geologists Bulletin*, 42(2): 387-430.

Adatte T., Bolle M.P., Kaenel E.D., Gawenda P., Winkler W. & von Salis K. (2000) - Climatic evolution from Paleocene to earliest Eocene inferred from clay-minerals: A transect from northern Spain (Zumaya) to southern (Spain, Tunisia) and southeastern Tethys margins (Israel, Negev). *GFF*, 122(1): 7-8.

Ali S., Gingras M. & Wilson W. (2021) - The shell-armoured trace fossil *Ereipichnus pickerillensis* from the Pliocene Moruga Formation, Trinidad: morphology and palaeoenvironment. *Ichnos*, 28(3): 243-252.

Allen P.A., Burgess P.M., Galewsky J. & Sinclair H.D. (2001) - Flexural-eustatic numerical model for drowning of the Eocene perialpine carbonate ramp and implications for Alpine geodynamics. *Geological Society of America Bulletin*, 113 (8): 1052 -1066.

Allmon W.D. (1988) - Ecology of Recent turritelline gastropods (Prosobranchia, Turritellidae): current knowledge and paleontological implications. *Palaios*, 3(3): 259-284.

Arena L., Giraldo-Gómez V.M., Baucon A., Piazza M., Papazzoni C.A., Pignatti J., Gandolfi A. & Briguglio A. (2024) - Short-term middle Eocene (Bartonian) paleoenvironmental changes in the sedimentary succession of Olivetta San Michele (NW Italy): the response of shallow-water biota to climate in NW Tethys. *Facies*, 70(4): 259-284.

Arni P. (1965) - L'évolution des Nummulitinae en tant que facteur de modification des dépôts littoraux. *Mémoires du BRGM* (Paris), 32: 7-20.

Baatsen M., Von der Heydt A.S., Hubert M., Kliphuis M.A., Bijl P.K., Sluijs A. & Dijkstra H.A. (2020) - The middle to late Eocene greenhouse climate modelled using the CESM 1.0.5. *Climate of the Past*, 16(6): 2573-2597.

Baccelle L. & Bosellini A. (1965) - Diagrammi per la stima visiva della composizione percentuale nelle rocce sedimentarie. *Annali dell'Università di Ferrara (Nuova Serie), Sezione 9, Scienze geologiche e paleontologiche*, 1(3): 59-62

Bassi D. (1998) - Coralline algal facies and their palaeoenvironments in the late Eocene of northern Italy (Calcare di Nago Trento). *Facies*, 39: 179-202.

Bassi D., Iryu Y., Humblet M., Matsuda H., Machiyama H., Sasaki K., Matsuda S., Arai K. & Inoue T. (2012) - Recent macroids on the Kikai jima shelf, Central Ryukyu Islands, Japan. *Sedimentology*, 59: 2024-2041.

Bassi D., Iryu Y., Humblet M., Matsuda H., Machiyama H., Sasaki K., Matsuda S., Arai K. & Inoue T. (2019) - Deep-water macroid beds of the Ryukyu Islands, Japan: encrusting acervulinids as ecosystem engineers. *Journal of Coastal Research*, 35: 463-466.

Basu H., Mahendra K., Paneerselvam S. & Chaki A. (2009) - Study of provenance characteristics and depositional history on the basis of U, Th and K abundances in the Gulcheru Formation, Cuddapah Basin in Tummalapalle-Somalollapalle areas, Cuddapah-Anantapur Districts, Andhra Pradesh. *Journal of the Geological Society of India*, 74(3): 318-328.

Baucon A. (2021) - Ichnoassociations, facies and depositional environments of a modern barrier-island: Ilha da Tavira (Ria Formosa, Portugal). *Palaeogeography, Palaeoclimatology, Palaeoecology*, 577: 110524.

Baucon A., Carvalho C.N.D., Felletti F., Tosadori G. & Antonelli A. (2021) - Small-world dynamics drove Phanerozoic divergence of burrowing behaviors. *Geology*, 49(6): 748-752.

Beavington-Penney S.J. & Racey A. (2004) - Ecology of extant nummulitids and other larger benthic foraminifera: applications in palaeoenvironmental analysis. *Earth-Science Reviews*, 67(3-4): 219-265.

Beavington-Penney S.J., Wright V.P. & Racey A. (2006) - The middle Eocene Seeb Formation of Oman: an investigation of acyclicity, stratigraphic completeness, and accumulation rates in shallow marine carbonate settings. *Journal of Sedimentary Research*, 76(10):1137-1161.

Bernardini F., Vinci G., Macovaz V., Baucon A., De Min A., Furlani S. & Smolić S. (2022) - Protohistoric stone disks from entrances and cemeteries of north-eastern Adriatic hill forts. *Documenta Praehistorica*, 49: 2-19.

Bessa J. (1995) - High-resolution outcrop gamma-ray spectrometry of the Lower Lias, southern Britain. Unpublished Ph.D. thesis, University of Oxford, Oxford, 247 pp. http://ora.ox.ac.uk/objects/uuid:901bed7b-e4e5-4791-8cf1-496430f7f9b1. Checked January 2024.

Bessa J.L. & Hesselbo S.P. (1997) - Gamma-ray character and correlation of the Lower Lias, SW Britain. *Proceedings of the Geologists' Association*, 108(2): 113-129.

Billings E. (1862) - New species of fossils from different parts of the Lower, Middle and Upper Silurian rocks of Canada. In: Billings E. (Ed.) - Palaeozoic Fossils, Vol. 1 (for 1861-1865): 96-168. Geological Survey of Canada, Montreal.

Bohaty S.M. & Zachos J.C. (2003) - Significant Southern Ocean warming event in the late middle Eocene. *Geology*, 31(11): 1017-1020.

Bohaty S.M., Zachos J.C., Florindo F. & Delaney M.L. (2009) - Coupled greenhouse warming and deep-sea acidification in the middle Eocene. *Paleoceanography*, 24(2): 1-16.

Boscolo-Galazzo F., Thomas E., Pagani M., Warren C., Luciani V. & Giusberti L - (2014). The middle Eocene climatic optimum (MECO): A multiproxy record of paleoceanographic changes in the southeast Atlantic (ODP Site 1263, Walvis Ridge). *Paleoceanography*, 29(12), 1143-1161.

Boussac J. (1912) - Études stratigraphiques sur le Nummulitique alpin: Mémoires pour servir à l'explication de la carte géologique détaillée de la France. Imprimerie nationale, Paris. France. 662 pp.

Brandano M. (2019) - The role of oceanographic conditions on Cenozoic carbonate platform drowning: insights from Alpine and Apennine foreland basins. *Terra Nova*, 31(2): 102-110.

Brandano M. & Tomassetti L. (2022) - MECO and Alpine orogenesis: constraints for facies evolution of the Bartonian nummulitic and *Solenomeris* limestone in the Argentina Valley (Ligurian Alps). *Sedimentology*, 69(1): 24-46.

Briguglio A. & Rögl F. (2018) - The Miocene (Burdigalian) Operculinids of Channa Kodi, Padappakkara, Southern India. *Palaeontographica A*, 312(1-4): 17-39.

Briguglio A., Seddighi M., Papazzoni C.A. & Hohenegger J. (2017) - Shear versus settling velocity of recent and fossil larger foraminifera: new insights on nummulite banks. *Palaios*, 32(5): 321-329.

Briguglio A., Giraldo-Gómez V.M., Baucon A., Benedetti A., Papazzoni C.A., Pignatti J., Wolfgring E. & Piazza M. (2024) - A middle Eocene shallow-water drowning ramp in NW Italy: from shoreface conglomerates to distal marl. *Newsletters on Stratigraphy*, 57(1): 37-63.

Bromley R.G. (1996) - Trace Fossils. Biology, Taphonomy and Applications. Chapman & Hall. London, Glasgow, Weinheim, New York, Tokyo, Melbourne, Madras. 361 pp. ISBN 0412 614804.

Bruguière J.G. (1792) - Camerine. Encyclopédie méthodique: Histoire naturelle des Vers, 1: 395-400.

Buatois L.A., Santiago N., Parra K. & Steel R. (2008) - Animal-substrate interactions in an early Miocene wave-dominated tropical delta: delineating environmental stresses and depositional dynamics (Tacata Field, eastern Venezuela). *Journal of Sedimentary Research*, 78(7): 458-479.

Cao L., Zhang Z., Zhao J., Jin X., Li H., Li J. & Wei X. (2021) - Discussion on the applicability of Th/U ratio for evaluating the paleoredox conditions of lacustrine basins. *International Journal of Coal Geology*, 248: 1-17.

Carbone F., Giammarino S., Matteucci R., Schiavinotto F. & Russo A. (1980) - Ricostruzione paleoambientale dell'affioramento nummulitico di Capo Mortola. *Annali dell'Università di Ferrara*, 9(6): 231-268.

Casoli E., Ricci S., Antonelli F., Perasso C.S., Belluscio A. & Ardizzone G. (2016) - Impact and colonization dynamics of the bivalve *Rocellaria dubia* on limestone experimental panels in the submerged Roman city of Baiae (Naples, Italy). *International Biodeterioration and Biodegradation*, 108: 9-15.

Cassidy J. (1981) - Techniques of field gamma-ray spectrometry. *Mineralogical Magazine*, 44(336): 391-398.

Chamley H. (2001) - Clay mineralogy. In: Encyclopedia of Ocean Science. Academic Press, 3900 pp.

Chou C., Chiang J.C.H., Lan C.W., Chung C.H., Liao Y.C. & Lee C.J. (2013) - Increase in the range between wet and dry season precipitation. *Nature Geoscience*, 6(4): 263-267.

Colletti A., Savinelli B., Di Muzio G., Rizzo L., Tamburello L., Fraschetti S. & Danovaro R. (2020) - The date mussel *Lithophaga lithophaga*: Biology, ecology and the multiple impacts of its illegal fishery. *Science of the Total Environment*, 744: 140866.

Coletti G., Mariani L., Garzanti E., Consani S., Bosio G., Vezzoli G., Hu X. & Basso D. (2021) - Skeletal assemblages and terrigenous input in the Eocene carbonate systems of the Nummulitic Limestone (NW Europe). *Sedimentary Geology*, 425: 1-23.

Cowan D.R. & Myers K.J. (1988) - Surface gamma ray logs: A correlation tool for frontier areas. *The American Association of Petroleum Geologists Bulletin*, 72: 634-636.

Crippa G., Baucon A., Felletti F., Raineri G. & Scarponi D. (2018) - A multidisciplinary study of ecosystem evolution through early Pleistocene climate change from the marine Arda River section, Italy. *Quaternary Research*, 89(2): 533-562.

Dallagiovanna G., Fanucci F., Pellegrini L., Seno S., Bonini L., Decarlis A., Maino M., Morelli D. & Toscani G. (2012a) - Note illustrative della Carta Geologica Foglio 257 - Dolceacqua: Regione Liguria, con contributi di Breda A., Vercesi P.L., Zizioli D., Cobianchi M., Mancin N., Papazzoni C.A. 75 pp. https://www.isprambiente.gov.it/Media/carg/note_illustrative/257_270_Dolceacqua_Ventimiglia.pdf. Checked January 2024.

Dallagiovanna G., Fanucci F., Pellegrini L., Seno S., Decarlis A., Maino M. & Toscani G. (2012b) - Carta Geologica alla scala 1: 25000 Foglio 257 "Dolceacqua" e Foglio 270 "Ventimiglia" con note ilustrative: Regione Liguria. http://www.cartografia.regione.liguria.it/templateFogliaRC.asp. Checked January 2024.

Day-Stirrat R.J., Hillier S., Nikitin A., Hofmann R., Mahood R. & Mertens G. (2021) - Natural gamma-ray spectroscopy (NGS) as a proxy for the distribution of clay minerals and bitumen in the Cretaceous McMurray Formation, Alberta, Canada. *Fuel*, 288: 119513.

De Graciansky P.C., Roberts D.G. & Tricart P. (2010) - The Western Alps, from rift to passive margin to orogenic belt: an integrated geoscience overview. Elsevier, 1st edition, 432 pp.

Decarlis A., Maino M., Dallagiovanna G., Lualdi A., Masini E., Seno S. & Toscani G. (2014) - Salt tectonics in the SW Alps (Italy-France): From rifting to the inversion of the European continental margin in a context of oblique convergence. *Tectonophysics*, 636: 293-314.

Deconinck J.F. (1992) - Sédimentologie des argiles dans le Jurassique-Crétacé d'Europe occidentale et du Maroc. Unpublished Ph.D. thesis, Université des Sciences et Technologies de Lille, Lille, 106 pp.

Deconinck J.F., Hesselbo S.P., Debuisser N., Averbuch O., Baudin F. & Bessa J. (2003) - Environmental controls on clay mineralogy of an Early Jurassic mudrock (Blue Lias Formation, southern England). *International Journal of Earth Sciences*, 92(2): 255-266,

Diester-Haass L., Robert C. & Chamley H. (1998) - Paleoproductivity and climate variations during sapropel deposition in the eastern Mediterranean Sea. *Proceedings-Ocean Drilling Program Scientific Results*, 160: 227-248.

Domènech R., De Gibert J.M. & Martinell J. (2001) - Ichnological features of a marine transgression: Middle Miocene rocky shores of Tarragona, Spain. *Geobios*, 34(1): 99-107.

Donovan S. (2003) - A new ichnospecies of *Gastrochaenolites* Leymerie from the Pleistocene Port Morant Formation of southeast Jamaica and the taphonomy of calcareous linings in clavate borings. *Ichnos*, 9(1-2): 61-66.

Donovan S.K. (2013) - A Recent example of the boring *Gastrochaenolites lapidicus* Kelly and Bromley and its producing organism in north Norfolk, eastern England. *Bulletin of the Mizunami Fossil Museum,* 39: 69-71.

Donovan S.K. & Hensley C. (2006) - *Gastrochaenolites* Leymerie in the Cenozoic of the Antillean region. *Ichnos*, 13(1): 11-19.

Dunham R.J. (1962) - Classification of carbonate rocks according to depositional texture. In: Hamm W.E. (Ed.) - Classifica-

tion of Carbonate Rocks - A Symposium. *AAPG Memoirs*, 1: 108-121.

Dypvik H. & Harris N.B. (2001) - Geochemical facies analysis of fine-grained siliciclastics using Th/U, Zr/Rb and (Zr+ Rb)/Sr ratios. *Chemical Geology*, 181(1-4): 131-146.

Edgar K.M., Wilson P.A., Sexton P.F., Gibbs S.J., Roberts A.P. & Norris R.D. (2010) - New biostratigraphic, magnetostratigraphic and isotopic insights into the Middle Eocene Climatic Optimum in low latitudes, *Palaeogeography, Palaeoclimatology, Palaeoecology*, 297, 670682, https://doi.org/10.1016/j.palaeo.2010.09.016, 2010.

Egger H., Briguglio A., Rögl F. & Darga R. (2013) - The basal Lutetian transgression on the tethyan shelf of the European craton (Adelholzen beds, Eastern Alps, Germany). *Newsletter on Stratigraphy*, 46(3): 287-301.

Egger H., Briguglio A., Rögl F. & Darga R. (2017) - Eocene stratigraphy of the Reichenhall basin (Eastern Alps, Austria, Germany). *Newsletter on Stratigraphy*, 50(3): 341-362.

Ekdale A.A. & Bromley R.G. (1983) - Trace fossils and ichnofabric in the Kjolby Gaard Marl, uppermost Cretaceous: Denmark. *Bulletin of the Geological Society of Denmark*, 31: 107-119.

Fabricius I.L., Fazladic L.D., Steinholm A. & Korsbech U. (2003) - The use of spectral natural gamma-ray analysis in reservoir evaluation of siliciclastic sediments: A case study from the Middle Jurassic of the Harald Field, Danish Central Graben. *Bulletin of the Geological Survey of Denmark and Greenland (GEUS)*, 1: 349-366.

Flügel E. (2012) - Microfacies of Carbonate Rocks: Analysis, Interpretation and Application. Springer Science & Business Media, Berlin, 984 pp.

Gandolfi A., Giraldo-Gómez V.M., Luciani V., Piazza M., Adatte T., Arena L., Bomou B., Fornaciari E., Frijia G., Kocsis L. & Briguglio A. (2023) - The Middle Eocene Climatic Optimum (MECO) impact on the benthic and planktic foraminiferal resilience from a shallow-water sedimentary record. *Rivista Italiana di Paleontologia e Stratigrafia*, 129(3): 629-651.

Gandolfi A., Giraldo-Gómez V.M., Luciani V., Piazza M., Brombin V., Crobu S., Papazzoni C.A., Pignatti J. & Briguglio A. (2024) - Unraveling ecological signals related to the MECO onset through planktic and benthic foraminiferal records along a mixed carbonate-siliciclastic shallow-water succession. *Marine Micropaleontology*, 190: 102388.

Gandolfi A., Giraldo-Gómez V.M., Arena L., Luciani V., Papazzoni C.A., Pignatti J., Piazza M., Kocsis L., Baumgartner C. & Briguglio A. (2025) - Diverse ecological responses of foraminifera to the Middle Eocene Climatic Optimum (MECO) in shallow-water settings (Provençal Domain, NW Italy). *Palaeogeography, Palaeoclimatology, Palaeoecology*, 661, 112697.

Gao Y., Xi D., Qin Z., Ma P. & Wang C. (2018) - Clay mineralogy of the first and second members of the Nenjiang Formation, Songliao Basin: Implications for paleoenvironment in the Late Cretaceous. *Science China Earth Sciences*, 61(3): 327-338.

Gèze B., Lanteaume M., Peyre Y., Vernet J. & Nestéroff W. (1968) - Carte géologique de la France au 1: 50.000: Feuille Menton-Nice, XXXVII-42 et 43. B.R.G.M. Orléans, 17 pp.

Giammarino S., Orezzi S., Piazza M. & Rosti D. (2009) - Evidence of syn-sedimentary tectonic activity in the "flysch di Ventimiglia" (Ligurian Alps foredeep basin). *Italian Journal of Geosciences*, 128 (2): 467-472.

Giammarino S., Fanucci F., Orezzi S., Rosti D., Morelli D., Cobianchi M., De Stefanis A., Di Stefano A., Finocchiaro F., Fravega P., Piazza M. & Vannucci G. (2010) - Note Illustrative della Carta Geologica d'Italia alla scala 1:50.000 - Foglio San Remo n. 258-271: ISPRA - Regione Liguria. 130 pp.

Gingras M.K., Maceachern J.A. & Dashtgard S.E. (2011) - Process ichnology and the elucidation of physico-chemical stress. *Sedimentary Geology*, 237(3-4): 115-134.

Giorgioni M., Jovane L., Rego E.S., Rodelli D., Frontalini F., Coccioni R., Catanzariti R. & Özcan E. (2019) - Carbon cycle instability and orbital forcing during the Middle Eocene Climatic Optimum. *Scientific Reports*, 9: 1-10.

Giraldo-Gómez V.M., Piazza M., Arena L., Baucon A., Gandolfi A., Papazzoni C.A., Pignatti J. & Briguglio A. (2024). A Paleogene mixed carbonate-siliciclastic system in the western Tethys: spectral gamma-ray as a tool for the reconstruction of paleoclimate and transgressive-regressive cycles. *Marine and Petroleum Geology*, 162: 106752.

Goeting S., Briguglio A., Eder W., Hohenegger J., Roslim A. & Kocsis L. (2018) - Depth distribution of modern larger benthic foraminifera offshore Brunei Darussalam. *Micropaleontology*, 64: 299-316.

Grabau A.W. (1904) - On the Classification of Sedimentary Rocks. American Geologist, Princeton University, 247 pp.

Hallock P. (1985) - Why are larger foraminifera large? *Paleobiology*, 11(2): 195-208.

Hallock P. (2000) - Symbiont-bearing foraminifera: harbingers of global change? In: Lee J.J. & Hallock P. (Eds.) - Advances in the Biology of Foraminifera. *Micropaleontology*, 46 (Suppl. 1): 95-148.

Hallock P. & Glenn E.C. (1986) - Larger foraminifera: a tool for paleoenvironmental analysis of Cenozoic carbonate depositional facies. *Palaios*, 1(1): 55-64.

Hallock P. & Schlager W. (1986) - Nutrient excess and the demise of coral reefs and carbonate platforms. *Palaios*, 1: 389-398.

Hammer Ø., Harper D.A. & Ryan P.D. (2001) - PAST: Paleontological statistics software package for education and data analysis. *Palaeontologia electronica*, 4(1): 1-9.

Held I.M. & Soden B.J. (2006) - Robust responses of the hydrological cycle to global warming. *Journal of Climate*, 19(21): 5686-5699.

Hesselbo S.P., Deconinck J.F., Huggett J.M. & Morgans-Bell H.S. (2009) - Late Jurassic palaeoclimatic change from clay mineralogy and gamma-ray spectrometry of the Kimmeridge Clay, Dorset, UK. *Journal of the Geological Society*, 166(6): 1123-1133.

Hohenegger J. & Briguglio A. (2012) - Axially oriented sections of nummulitids. A tool to interpret larger benthic foraminiferal deposits. *Journal of Foraminiferal Research*, 42(2): 134-142.

Hohenegger J., Kinoshita S., Briguglio A., Eder W. & Wöger J. (2019) - Lunar cycles and rainy seasons drive growth and reproduction in nummulitid foraminifera, important producers of carbonate buildups. *Scientific Reports*, 9(1): 8286.

Hottinger L. (1983) - Processes determining the distribution of larger foraminifera in space and time. *Utrecht Micropaleontological Bulletins*, 30: 239-253.

Hottinger L. (1997) - Shallow benthic foraminiferal assemblages as signals for depth of their deposition and their limitations. *Bulletin de la Société géologique de France*, 168(4), 491-505.

Hottinger L. (2006) - The depth-depending ornamentation of some lamellar-perforate foraminifera. *Symbiosis*, 42: 141-151.

Hölder H. (1989) - Spuren auf der Spur. Palichnologische und verwandte Notizen über *Teredolites*, *Entobia*, *Nummipera* nov. gen. und einiges andere. *Münsterische Forschungen zur Geologie und Paläontologie*, 69: 13-30.

Jach R., Machaniec E. & Uchman A. (2012) - The trace fossil *Nummipera eocenica* from the Tatra Mountains, Poland. Morphology and palaeoenvironmental implications. *Lethaia*, 45(3): 342-355.

Kalvoda J.I.Ø.Í., Bábek O.N.D.Ø.E.J., Devuyst F.X. & Sevastopulo G.D. (2011) - Biostratigraphy, sequence stratigraphy and gamma-ray spectrometry of the Tournaisian-Viséan boundary interval in the Dublin Basin. *Bulletin of Geosciences*, 86(4): 683-706.

Kennedy M.J. & Wagner T. (2011) - Clay mineral continental amplifier for marine carbon sequestration in a greenhouse ocean. *Proceedings of the National Academy of Sciences of the United States of America*, 108(24): 9776-9781.

Kleiber G.W. (1991) - Nummuliten der paläogenen Tethys in Axialschnitten. *Tübinger Mikropaläontologische Mitteilungen*, 9: 1-262.

Knaust D. (2017) - Atlas of trace fossils in well core: Appearance,

Taxonomy and Interpretation: Springer, Germany, 1st edition, 224 pp.

Knaust D. (2018) - The ichnogenus *Teichichnus* Seilacher, 1955. *Earth-Science Reviews*, 177: 386-403.

Knaust D. (2021) - Ichnofabric. In: Encyclopedia of Geology. Elsevier, 520-531.

Koptíková L., Bábek O., Hladil J., Kalvoda J. & Slavík L. (2010) - Stratigraphic significance and resolution of spectral reflectance logs in Lower Devonian carbonates of the Barrandian area, Czech Republic; a correlation with magnetic susceptibility and gamma-ray logs. *Sedimentary Geology*, 225(3-4): 83-98.

Kouamelan K.S., Zou C., Wang C., Assie K.R., Peng C., Mondah O.R. & Brantson E.T. (2020) - Multifractal characterization of the Coniacian-Santonian OAE 3 in lacustrine and marine deposits based on spectral gamma ray logs. *Scientific Reports*, 10(1): 1-22.

Kövecsi S.A., Less G., Ples G., Bindiu-Haitonic R., Briguglio A., Papazzoni C.A. & Silye L. (2022) - *Nummulites* assemblages, biofabrics and sedimentary structures: The anatomy and depositional model of an extended Eocene (Bartonian) nummulitic accumulation from the Transylvanian Basin (NW Romania). *Palaeogeography, Palaeoclimatology, Palaeoecology*, 586: 110751.

Lanteaume M. (1968) - Contribution à l'étude géologique des Alpes Maritimes franco-italiennes. Mémoires pour servir à l'explication de la carte géologique détaillée de la France. 405 pp.

Lokier S.W., Wilson M.E., & Burton L.M. (2009) - Marine biota response to clastic sediment influx: a quantitative approach. *Palaeogeography, Palaeoclimatology, Palaeoecology*, 281(1-2): 25-42.

Loughlin N.J. & Hillier R.D. (2010) - Early Cambrian *Teichichnus*-dominated ichnofabrics and palaeoenvironmental analysis of the Caerfai Group, Southwest Wales, UK. *Palaeogeography, Palaeoclimatology, Palaeoecology*, 297(2): 239-251.

Marini M., Patacci M., Felletti F., Decarlis A. & McCaffrey W. (2022) - The erosionally confined to emergent transition in a slope-derived blocky mass-transport deposit interacting with a turbidite substrate, Ventimiglia Flysch Formation (Grès d'Annot System, north-west Italy). *Sedimentology*, 69(4): 1675-1704.

Marvel K. & Bonfils C. (2013) - Identifying external influences on global precipitation. *Proceedings of the National Academy of Sciences*, 110(48): 19301-19306.

Mendoza-Rodríguez G., Buatois L.A., Rincón-Martínez D., Mángano M.G. & Baumgartner-Mora C. (2020) - The armored burrow *Nummipera eocenica* from the upper Eocene San Jacinto Formation, Colombia: morphology and paleoenvironmental implications. *Ichnos*, 27(2): 81-91.

Messaoud J.H., Thibault N., Bomou B., Adatte T., Monkenbusch J., Spangenberg J.E. & Yaich C. (2021) - Integrated stratigraphy of the middle-upper Eocene Souar Formation (Tunisian dorsal): Implications for the Middle Eocene Climatic Optimum (MECO) in the SW Neo-Tethys. *Palaeogeography, Palaeoclimatology, Palaeoecology*, 581: 1-18.

Mikuláš R. & Žítt J. (2003) - The ichnogenus *Gastrochaenolites* and its tracemakers from firmgrounds of the Bohemian Cretaceous Basin (Czech Republic). *Ichnos*, 10(1): 15-23.

Molina E., Torres-Silva A.I., Coric S. & Briguglio A. (2016) - Integrated biostratigraphy across the Eocene/Oligocene boundary at Noroña, Cuba, and the question of the extinction of orthophragminids. *Newsletters on Stratigraphy*, 49(1): 27-40.

Montfort P. (1808) - Conchyliologie systématique et classification méthodique des coquilles. Paris: Schoell, 1: 1-409.

Morelli D., Locatelli M., Corradi N. Cianfarra P., Crispini L., Federico L. & Migeon S. (2022) - Morpho-structural setting of the Ligurian Sea: The role of structural heritage and neotectonic inversion. *Journal of Marine Science and Engineering*, 10(9): 1-24.

Moussavou B.M. (2015) - Bivalves (Mollusca) from the Coniacian-Santonian Anguille Formation from Cap Esterias, northern Gabon, with notes on paleoecology and paleobiogeography. *Geodiversitas*, 37(3): 315-324.

Mueller P., Langone A., Patacci M., & Di Giulio A. (2018) - Detrital signatures of impending collision: The deep-water record of the Upper Cretaceous Bordighera Sandstone and its basal complex (Ligurian Alps, Italy). *Sedimentary Geology*, 377: 147-161.

Myers K.J. (1987) - Onshore outcrop gamma ray spectrometry as a tool in sedimentological studies: Unpublished PhD thesis, University of London, London, UK, 310 pp.

Myers K.J. & Wignall P.B. (1987) - Understanding Jurassic organic-rich mudrocks-new concepts using gamma-ray spectrometry and palaeoecology: examples from the Kimmeridge Clay of Dorset and the Jet Rock of Yorkshire. In: J.K. Leggett, and G.G. Zuffa (Eds.) - Marine clastic sedimentology: Concepts and case studies. Springer: 172-189.

Paredes J.M., Giordano S.R., Olazabál S.X., Valle M.N., Allard J.O., Foix N. & Tunik M.A. (2020) - Climatic control on stacking and connectivity of fluvial successions: upper Cretaceous Bajo Barreal Formation of the Golfo san Jorge basin, Patagonia. *Marine and Petroleum Geology*, 113: 104116.

Pemberton S.G. & Frey R.W. (1982) - Trace fossil nomenclature and the *Planolites-Palaeophycus* dilemma. *Journal of Paleontology*, 56(4): 843-881.

Peris Cabré S., Valero L., Spangenberg J.E., Vinyoles A., Verité J., Adatte T., Maxime Tremblin M., Watkins S., Sharma N., Garcés M., Puigdefàbregas C. & Castelltort S. (2023) - Fluvio-deltaic record of increased sediment transport during the Middle Eocene Climatic Optimum (MECO), Southern Pyrenees, Spain. *Climate of the Past*, 19(3): 533-554.

Perotti E., Bertok C., d'Atri A., Martire L., Piana F. & Catanzariti R. (2012) - A tectonically-induced Eocene sedimentary mélange in the West Ligurian Alps, Italy. *Tectonophysics*, 568: 200-214.

Quirein J.A., Gardner J.S. & Watson J.T. (1982) - Combined natural gamma ray spectral/litho-density measurements applied to complex lithologies. *SPE Annual Technical Conference and Exhibition*, 11143: 1-4.

Ravenne C., Riche P., Tremolieres, P. & Vially R. (1987) - Sédimentation et tectonique dans le bassin marin Eocène supérieur-Oligocène des Alpes du Sud. *Revue de l'Institut français du Pétrole*, 42(5): 529-553.

Rego E.S., Jovane L., Hein J.R., Sant'Anna L.G., Giorgione M., Rodelli D. & Özcan E. (2018) - Mineralogical evidence for warm and dry climatic conditions in the Neo-Tethys (eastern Turkey) during the Middle Eocene. *Palaeogeography, Palaeoclimatology, Palaeoecology*, 501: 45-57.

Renema W. (2018) - Terrestrial influence as a key driver of spatial variability in large benthic foraminiferal assemblage composition in the Central Indo-Pacific. *Earth-Science Reviews*, 177: 514-544.

Reolid M., Iwanczuk J., Mattioli E., Abad I. & Özcan E. (2020) - Integration of gamma ray spectrometry, magnetic susceptibility and calcareous nannofossils for interpreting environmental perturbations: an example from the Jenkyns Event (lower Toarcian) from South Iberian Palaeomargin (Median Subbetic, SE Spain). *Palaeogeography, Palaeoclimatology, Palaeoecology*, 560: 110031.

Robert H. & Chamley H. (1991) - Development of Early Eocene warm climates, as inferred from clay mineral variations in oceanic sediments. *Palaeogeography, Palaeoclimatology, Palaeoecology*, 89(4): 315-331.

Roslim A., Briguglio A., Kocsis L., Ćorić S. & Gebhardt H. (2019) - Large rotaliid foraminifera as biostratigraphic and palaeoenvironmental indicators in northwest Borneo: An example from a late Miocene section in Brunei Darussalam. *Journal of Asian Earth Sciences*, 170: 20-28.

Ruffell A. & Kürschner W.M. (2020) - Sediment cyclicity and the Carnian Pluvial Episode: Evidence from spectral gamma-ray logging of the Mercia Mudstone Group, SW England.

Boletín Geológico y Minero, 131(2): 231-242.

Ruffell A. & Worden R. (2000) - Palaeoclimate analysis using spectral gamma-ray data from the Aptian (Cretaceous) of southern England and southern France. *Palaeogeography, Palaeoclimatology, Palaeoecology*, 155(3-4): 265-283.

Sayer Z.R. (1995) - The Nummulitique: carbonate deposition in a foreland basin setting; Eocene, French alps. Unpublished PhD Thesis. Durham University. Durham, UK, 351 pp. http://ethe ses.dur.ac.uk/6103/. Checked January 2025.

Schaub H. (1981) - Nummulites et Assilines de la Téthys paléogène. Taxinomie, phylogenèse et biostratigraphie. *Schweizerische Paläontologische Abhandlungen*, 104: 1-236.

Scheibner C., Rasser M.W. & Mutti M. (2007) - The Campo section (Pyrenees, Spain) revisited: Implications for changing benthic carbonate assemblages across the Paleocene-Eocene boundary. *Palaeogeography, Palaeoclimatology, Palaeoecology*, 248(1-2): 145-168.

Schlumberger (1997) - Log Interpretation Charts: Schlumberger Wireline & Testing. Houston, Texas, USA - Schlumberger Ltd. 193 pp .

Schnyder J., Ruffell A., Deconinck J.F. & Baudin F. (2006) - Conjunctive use of spectral gamma-ray logs and clay mineralogy in defining late Jurassic-early Cretaceous palaeoclimate change (Dorset, UK). *Palaeogeography, Palaeoclimatology, Palaeoecology*, 229(4): 303-320.

Seddighi M., Briguglio A., Hohenegger J. & Papazzoni C.A. (2015) - New results on the hydrodynamic behaviour of fossil *Nummulites* tests from two nummulite banks from the Bartonian and Priabonian of northern Italy. *Bollettino della Società Paleontologica Italiana*, 54(2): 103-116.

Seilacher A. (1955) - Spuren und Fazies im Unterkambrium. In: Schindewolf O.H. & Seilacher A. (Eds.) - Beiträge zur Kenntnis des Kambriums in der Salt Range (Pakistan). *Akademie der Wissenschaften und der Literatur zu Mainz, Abhandlung Mathematisch-Naturwissenschaftliche* Klasse 1955(10): 373-399.

Sharma N., Spangenberg J.E., Adatte T., Vennemann T., Kocsis L., Vérité J. & Castelltort S. (2024) - Middle Eocene Climatic Optimum (MECO) and its imprint in the continental Escanilla Formation, Spain. *Climate of the Past*, 20(4): 935-949.

Sinclair H.D. (1997) - Tectonostratigraphic model for underfilled peripheral foreland basins: An Alpine perspective. *Bulletin of the Geological Society of America*, 109(3): 324-346.

Sinclair H.D., Sayer Z.R. & Tucker M.E. (1998) - Carbonate sedimentation during early foreland basin subsidence. the Eocene succession of the French Alps. *Geological Society, London, Special Publications*, 149(1): 205-227.

Slatt R.M., Jordan D.W., D'Agostino A.E. & Gillespie R.H. (1992) - Outcrop gamma-ray logging to improve understanding of subsurface well log correlations. *Geological Society, London, Special Publications*, 65(1): 3-19.

Sluijs A., Van Roij L., Harrington G.J., Schouten S., Sessa J.A., Levay L.J. & Slomp C.P. (2014) - Warming, euxinia and sea level rise during the Paleocene-Eocene Thermal Maximum on the Gulf Coastal Plain: implications for ocean oxygenation and nutrient cycling. *Climate of the Past*, 10(4): 1421-1439.

Sowerby J. (1840) - In Sykes, W. H.: A notice respecting some fossils collected in Cutch, by Capt. Walter Smee, of the Bombay Army. *Transactions of the Geological Society of London*. ser. 2, 5(3): 715-719.

Spofforth D.J.A., Agnini C., Pälike H., Rio D., Fornaciari E., Giusberti L., Luciani V., Lanci L. & Muttoni G. (2010) - Organic carbon burial following the middle Eocene climatic optimum in the central western Tethys. *Paleoceanography*, 25(3): 1-11.

Taylor A., Goldring R. & Gowland S. (2003) - Analysis and application of ichnofabrics. *Earth-Science Reviews*, 60(3-4): 227-259.

Tomás S., Frijia G., Bömelburg E., Zamagni J., Perrin C. & Mutti M. (2016) - Evidence for seagrass meadows and their response to paleoenvironmental changes in the early Eocene (Jafnayn Formation, Wadi Bani Khalid, N Oman). *Sedimentary Geology*, 341: 189-202.

Tomassetti L., Benedetti A. & Brandano M. (2016) - Middle Eocene seagrass facies from Apennine carbonate platforms (Italy). *Sedimentary Geology*, 335: 136-149.

Torres-Silva A.I., Hohenegger J., Coric S., Briguglio A. & Eder W. (2017) - Biostratigraphy and evolutionary tendencies of Eocene heterostegines in western and central Cuba based on morphometric analyses. *Palaios*, 32(1): 44-60.

Torres-Silva A.I., Eder W., Hohenegger J. & Briguglio A. (2019) - Morphometric analysis of Eocene nummulitids in western and central Cuba: taxonomy, biostratigraphy and evolutionary trends. *Journal of Systematic Palaeontology*, 17(7): 557-595.

Toscano A.G., Lazo D.G. & Luci L. (2018) - Taphonomy and paleoecology of Lower Cretaceous oyster mass occurrences from west-central Argentina and evolutionary paleoecology of gregariousness in oysters. *Palaios*, 33(6): 237-255.

Uchman A. & Wetzel A. (2011) - Deep-sea ichnology: the relationships between depositional environment and endobenthic organisms. *Developments in Sedimentology*, 63: 517-556.

Varrone D. (2004) - Le prime fasi di evoluzione del bacino di avanfossa alpino: la successione Delfinese cretacico-eocenica, Alpi Marittime: Unpublished PhD. thesis, Tesi di Dottorato, Dip. Scienze della Terra, Università degli Studi di Torino. Torino, Italia, 145 pp.

Varrone D. & Clari P. (2003) - Évolution stratigraphique et paléoenvironnementale de la Formation à Microcodium et des Calcaires à Nummulites dans les Alpes Maritimes franco-italiennes. *Geobios*, 36: 775-786.

Varrone D. & d'Atri A. (2007) - Acervulinid macroid and rhodolith facies in the Eocene Nummulitic Limestone of the Dauphinois Domain (Maritime Alps, Liguria, Italy). *Swiss Journal of Geosciences*, 100(3): 503-515.

Varrone D. & Decrouez D. (2007) - Eocene larger foraminiferal biostratigraphy in the southernmost Dauphinois Domain (Maritime Alps, France-Italy border). *Rivista Italiana di Paleontologia e Stratigrafia*, 113 (2): 257-267.

Ward J.H. (1963) - Hierarchical grouping to optimize an objective function. *Journal of the American Statistical Association*, 58(301): 236-244.

Wetzel A. & Uchman A. (1998) - Deep-sea benthic food content recorded by ichnofabrics; a conceptual model based on observations from Paleogene flysch, Carpathians, Poland. *Palaios*, 13(6): 533-546.

Wignall P.B. & Twitchett R.J. (1996) - Oceanic anoxia and the End Permian mass extinction. *Science*, 272(5265): 1155-1158.

Zachos J.C., Dickens G.R. & Zeebe R.E. (2008) - An early Cenozoic perspective on greenhouse warming and carbon-cycle dynamics. *Nature*, 451(7176): 279-283.

Zachos J., Pagani M., Sloan L., Thomas E. & Billups K. (2001) - Trends, rhythms, and aberrations in global climate 65 Ma to present. *Science*, 292(5517): 686-693.

Žítt J & Mikuláš R. (2006) - Substrate of bivalve borers as recorded on phosphatic fills of *Gastrochaenolites*, palaeoenvironmental context (Bohemian Cretaceous Basin, Czech Republic). *Ichnos*, 13(3). 191-198.